Sudan University of Science and Technology

College of Graduate Studies

Tracking of Refractive Index variation of (Polymethyl Methacrylate after irradiated by femtosecond Laser)

تتبع التغير الذي يطرأ على معامل الانكسار للهولي ميثايل ميثاكريلات بواسطة الليزرالنبضي

A Thesis Submitted in Fulfilment for the Requirements of the Degree of Doctor of Philosophy in Laser Application in Physics

By

Abdel Rahman Abdel Bari Mohamed

Supervisor:

Prof. Kais A. M. Al Naimee

Co- Supervisor:

Dr. Kasim Al Hity

August-2017

I

Dedication

This thesis is dedicated to:

Soul of my parents (mother and father), and grandparents.

My wife Rehab my best friend through everything.

My sons and daughters.

My brothers and sisters.

الآية

بِسْمِ ٱللَّهِ ٱلرَّحْمَٰنِ ٱلرَّحِيمِ

ٱللَّهُ لَآ إِلَٰهَ إِلَّا هُوَ ٱلْحَىُّ ٱلْقَيُّومُ لَا تَأْخُذُهُۥ سِنَةٌ وَلَا نَوْمٌ لَّهُۥ مَا فِى ٱلسَّمَٰوَٰتِ وَمَا فِى ٱلْأَرْضِ مَن ذَا ٱلَّذِى يَشْفَعُ عِندَهُۥٓ إِلَّا بِإِذْنِهِۦ يَعْلَمُ مَا بَيْنَ أَيْدِيهِمْ وَمَا خَلْفَهُمْ وَلَا يُحِيطُونَ بِشَىْءٍ مِّنْ عِلْمِهِۦٓ إِلَّا بِمَا شَآءَ وَسِعَ كُرْسِيُّهُ ٱلسَّمَٰوَٰتِ وَٱلْأَرْضَ وَلَا يَـُٔودُهُۥ حِفْظُهُمَا وَهُوَ ٱلْعَلِىُّ ٱلْعَظِيمُ ﴿٢٥٥﴾

صدق الله العظيم

Acknowledgement

There are many people I would like to thank for their support that made this work possible. First, I thank my supervisor, Prof. Kais Al Naimee, who gave me the opportunity to do research in his group, also for the valuable input and guidance I have received.

I am also grateful to my first co-supervisor, Dr. Kasim Al Hity for teaching us fundamental courses in optics and laser. Dr. Abdel Moneim M. Awad , for his assistance, guidance and encouragement on my scientific work and during writing my thesis, also for teaching us laser physics course.

I would like to express my gratitude to the Institute of Laser (SUST) and its Dean Dr. Ali Marouf

Many thanks also go to the Photon Science Institute, University of Manchester, Manchester, UK,

In addition, I thank my colleagues in Prof. Kais group for it has been a great pleasure working with them for all these years.

Finally, very special thanks for my wife and my children, whom make me stronger than I would be without them.

Abstract

This research is aim to modify the subsurface of poly methyl methacrylate (PMMA) and create diffraction grating by means of ultra short UV laser(Ti:Saphire) with pulse duration of 250 femto-second laser, wavelength of about 387nm, output beam from the system is 0.105 µJ, the grating writing (scanning) speed is 1.25 mm/s, the grating period is 40µm.

The experimental result of interferometric patterns (with Mach-Zehnder interferometer) for the samples before and after radiation showed that the discontinuity of fringes pattern is due to the irradiated zone inside the sample because of photo- thermal and optical density changes in (PMMA) subsurface caused by laser radiation.

It was found that when uses matlab programme for the two digitized interferograms images the refractive index map obtain, the variation in Δn is be clear along x-axis in this figure, the high peak of Δn occurs at midpoint of focusing Coherent Legend Ti: Sapphire laser to PMMA sample.

The results above showed that laser direct writing technique is easy to change the optical characterizations of the materials, produce PMMA diffraction grating as well as high quality.

This mechanism is strongly dependant on the optical properties of the material and is recommended to be studied experimentally and theoretically in the future.

المستخلص

الهدف من هذه الدراسة هو تعديل السطح الداخلي لمادة البولي ميثايل ميثاكرايلايت، وإختراع محزوز الحيود باستخدام الليزر النبضي ذو الطاقة العالية، زمن النبضة 250 فيمتو ثانية، وطول موجي 387 نانومتر، وطاقة 0.105 مايكرو جول، وتباعد بين الحزوز 40 مايكرو متر، و بسرعة مسح 1.25 مليمتر لكل ثانية.

أظهرت النتائج للعينات المشععة وغير المشععة بعد عرضها علي مقياس تداخل الامواج ماخزندر أن هناك تغيير في مسار الأهداب للعينات المشععة مما يشيرٍ إلي تغيير في الخواص الضوئية للعينة بما في ذلك تغيير في معامل الإنكسار.

وأكَدت نتائج برنامج الماتلاب عند إدخال صور المطياف البصري للعينات قبل وبعد التشعيع بتغير معامل الإنكسار، وان هذا التغير يصل قمته في منطقة مركز الشعاع .

ووجد من النتائج اعلاه انه من السهل جدا إمكانية الحصول علي محزوز حيود بوليمري وبالمواصفات المطلوبة

ان تقنية النقش علي المواد بواسطة الليزر تعتمد إعتماد كلي علي الخواص الضوئية للمادة ويجب عمل المزيد من الدراسات العملية والنظرية في المستقبل لتدعم البحث العلمي في هذا المجال.

Table of contents

Chapter 1: Introduction and Literature Review

Chapter 2: Theoretical background

Chapter 3: Experimental part

Chapter 4: Results and Discussion

List of Figures

List of Tables

List of Abbreviations

3-D	Three Dimensions
AFM	Atomic-force microscopy
APS	Air Plasma Sprayed
BBO	Beta Barium Borate
CASR	Coherent Anti-Stokes Raman
CCD	Charge-Coupled Devices
CW	Continuous-Wave
DSC	3 Differential Scanning Calorimetry
E_{bg}	band gap
EDS	Energy-Dispersive X-ray Spectroscopy
fs	Femto-second
HAZ	heat affected zone
IR	Infra-red
LDPE	low density polyethylene
LDW	Laser Direct Writing
LDW-	laser direct write subtraction
LDW+	laser direct-write addition
LDWM	laser direct-write modification
LIBWE	laser-induced backside wet etching
LIFT	laser induced forward transfer
$LiNbO_3$	Lithium Niobate
LO	longitudinal-optical
ND	natural density

Nd:YAG	neodymium-doped yttrium aluminium garnet; $Nd:Y_3Al_5O_{12}$
NIR	near infrared
PDMS	poly dimethyl siloxane
PDMS	Poly dimethylsiloxane
PMA	poly(methyl acrylate)
PMMA	poly(methyl methacrylate)
PMT	Photomultiplier Tubes
POF	polymer optical fibre
ps	pico-second
PS	polystyrene
PVA	poly vinylalcohol
SFF	solid free-form fabrication
SHG	Second-harmonic-generation
SLS	selective laser sintering
T_e	electron temperature
Ti: Sapphire	titanium–sapphire
T_m	equilibrium melting point
UV	ultraviolet
Vis	visible
WDM	wavelength-division multiplexing
XRD	X-ray diffraction

Chapter One

Introduction and Literature Review

1.1. Introduction:

The geometrical model of the propagation of light was derived from the basic equations of electromagnetic theory, and it was shown that, with certain approximations, variations of intensity in a beam of light can be described in terms of changes in the cross-sections area of a tube of rays. When two or more light beams are superposed, the distribution of intensity can no longer in general be described in such a simple manner. Thus if light from a source is divided by suitable apparatus into two beams which are then superposed, the intensity in the region of superposition is found to vary from point between maxima which exceed the sum of the intensities in the beams, and minima which may be zero. This phenomenon is called interference. We shall see shortly that the superposition of beams of strictly monochromatic light always gives rise to interference. However, light produced by a real physical source is never strictly monochromatic but, as we learn from atomistic theory, the amplitude and phase undergo irregular fluctuations much too rapid for the eye or an ordinary physical detector to follow. If the two beams originate in the same source, the fluctuations in the two beams are in general correlated, and the beams are said to be completely or partially coherent depending on whether the correlation is complete or partial. In beams from different sources, the fluctuations are completely uncorrelated, and the beams are said to be mutually incoherent. When such beams from different sources are superposed, no interference is observed under ordinary experimental conditions, the total intensity being everywhere the sum of the intensities of the intensities of the individual beams. The 'degree of correlation' that exists between the fluctuations in two light beams determines, and conversely is revealed by, the

'depth of modulation' of the interference pattern to which the beams give rise on superposition. There are two general methods of obtaining beams from a single beam of light, and these provide a basis for classifying the arrangements used to produce interference. In one the beam is divided by passage through apertures placed side by side. This method, which is called division of wave front, is useful only with sufficiently small sources. Alternatively the beam is divided at one or more partially reflecting surfaces, at each of which part of the light is reflected and part transmitted. This method is called division of amplitude, it can be used with extended sources, and so the effects may be of greater intensity than with division of wave front. In either case, it is convenient to consider separately the effects which result from the superposition of two beams (two beam interference).

In recent year, there has been much interest in applying focused femto-second laser pulses at high repetition rate to induce various localized microstructures near the focal point of laser beam in transparent material. Focused femto-second laser pulses induce structural changes inside the transparent material, such as glass and polymers, due to nonlinear absorption at high peak powers. The induced refractive index change can be used to fabricate the three –dimensional microstructures and optical devices. (*A. Baum et al, (2007)*). Several photonic structures have been realized in glass crystals (Davis, K.M., *et al*., 1996; Miura, K., *et al*., 1997; Homoelle, D., *et al*., 1999; Qiu, J., *et al*., 2000; Qiu, J., *et al*., 2001; Luo, L., *et al*., 2002).

Femtosecond laser micromachining was first demonstrated in 1994, when a femtosecond laser was used to ablate micrometresized features on silica and silver surfaces. In less than ten years the resolution of surface ablation has improved to enable nanometre-scale precision. Several review articles are available on femtosecond lasers, nonlinear processes, optical

breakdown, surface micromachining and the history of femtosecond laser micromachining.

PMMA based polymer optical fibre (POF) and optical components are inert, inexpensive, rugged, and thus ideal for disposable sensor devices in clinical, biological and chemical applications. In-fibre gratings formed in POF have advantages as sensors because the bulk thermo-optic, electro-optic and strain sensitivities of polymers are up to 10 times those of glass. The photomodification and ablation of PMMA based on linear absorption of UV continuous wave and excimer laser are well studied processes , however, their low penetration depth limits 3D applications. Ultra-short pulsed laser refractive index modification of PMMA to date employs the nonlinear absorption of the fundamental Ti:Sapphire laser wavelength around 800 nm. Whereas other refractive index structuring methods often require photosensitization, Scully *et al.* showed that commercial grade PMMA can be readily photomodified by fs irradiation , a clean procedure requiring neither pre-nor post-processing. Low dose excimer laser experiments showed that nanosecond photochemical processes in PMMA produce positive as well as negative refractive index changes . "Initial wave guide structures in PMMA using 800 nm, fs laser pulses reported differing results about the sign of the refractive index change" [Taranu et al.(2010)].

Fabrication of photonic structures (waveguides and gratings) in bulk polymethyl methacrylate (PMMA) and polymer using femtosecond laser irradiation, can be optimised by selecting wavelength, pulse length and repetition rate of the laser irradiation ,[Taranu A. et al (2010), Scully, Jones and Jaroszynski, (2003), Baum et al (2008), Liang, et al (2010] .Optimal conditions for permanent refractive index modification without doping for photosensitivity are facilitated by studies of the associated photochemistry. Raman mapping was used to study both laser induced photochemical and non-chemical optical and material density modification effect, both of which cause refractive index changes.[Baum, et al (2007), Baum et al (2010)]. Direct observation of femto-second light-induced refractive index changes is thus necessary for

understanding and controlling, namely, scanning speed, laser energy and laser pulse duration [Baum A., et al (2008)]. These parameters can be changed independently but their effects are unavoidably superposed upon each other. Phase contrast microscopy has been used for optical analysis of phase grating structures [D. Kip, (1998)].

Optical waveguide structures fabricated by using femtosecond laser direct-write (FLDW) techniques are promising devices in the field of optical signal management and amplification. The fabrication of these devices is quick and simple, the technique can be applied to a range of dielectric materials such as glasses and polymers, and it has genuinely three-dimensional capabilities offering unique opportunities for the construction of complex optical components in passive and active materials. The FLDW technique relies on the light–material interaction at the focus of a tightly focused femtosecond laser beam where, in most glassy materials, the energy at focus causes localized densification leading to a positive change in the refractive index, a process that does not require material photosensitivity. [Davis K. M. et al (1996), Saliminia A. et al (2003)].

Many novel and interesting devices have been made using femtosecond laser direct writing; these include 1-to-N splitters in two or more dimensions, interferometers, and miniature gain volumes. [Liu J. R. et al, (2005), Florea C., Winick K. A. and Lightwave J. (2003), Della Valle G., et al, (2005)].

However, the technique has lacked the integration of an important functional form, namely, grating structures. In other buried and rib waveguide devices, gratings manufactured by electron-beam lithography and interference

photolithography have been used to great effect to fabricate wavelength filters and laser mirrors. [W. H. Wong W. H., Pun E. Y. B., and K. S. Chan K. S., (2003). Yliniemi S., J. Albert J., Q. Wang Q., and S. Honkanen S., (2006)].

Interferometry is an important investigative technique in which electromagnetic waves are superimposed in order to extract information about the waves. An instrument used to interfere waves is called an interferometer. It is an important investigative technique in the fields of astronomy, fiber optics, engineering metrology, optical metrology, oceanography, seismology, quantum mechanics, nuclear and particle physics, plasma physics, remote sensing and biomolecular interactions.

Interferometry makes use of the principle of superposition to combine separate waves in a way that will cause the result of their combination to have some meaningful property that is diagnostic of the original state of the waves. This works because when two waves with the same frequency combine, the resulting pattern is determined by the phase difference between the two waves—waves that are in phase will undergo constructive interference while waves that are out of phase will undergo destructive interference. Most interferometers use light or some other form of electromagnetic wave [Pal, Bishnu P. (1992)].

Typically a single incoming beam of coherent light will be split into two identical beams by a grating or a partial mirror. Each of these beams will travel a different route, called a path, until they are recombined before arriving at a detector. The path difference, the difference in the distance traveled by each beam, creates a phase difference between them. It is this introduced phase difference that creates interference pattern between the initially identical waves. If a single beam has been split along two paths then the phase difference is diagnostic of anything that change s the phase along the paths. This could be a physical change in the path length itself or a change in the refractive index along the path.

The refractive index of a material is an important optical parameter since it exhibits the optical properties of the material. [Shyam Singh, 2002].

It is a measure of how much the speed of light (or other forms of waves) is reduced inside a medium compared to the speed of light in a vacuum. Light propagates more slowly through media with higher refractive indices. Because of this, the optical path of light is equal to the physical distance times the refractive index of the medium, and therefore an optical distance is not the same as the physical distance. This property can be used in conjunction with a Michelson interferometer to measure the refractive index of a material with a known thickness. Its values are often required to interpret various types of spectroscopic data. The refractive index coefficients are important parameters in the design of a solid state laser. The adulteration problem is increasing day by day and hence simple, automatic and accurate measurement of the refractive index of the materials is of great importance these days. Quick measurements of refractive indices using simple techniques and refractometers can help controlling adulteration of liquids of common use to a greater extent. Sensitive determination of the refractive indices of certain materials is very important in many fields of research such as material analysis and environmental pollution monitoring.

1.2. Literature review

Florea *et al* (2003), reported both straight and curved waveguides written in a variety of silicate glasses using near-IR femtosecond laser pulses. Writing parameters are identified that produce waveguides that support only a single mode and yield smooth-mode profiles. The laser pulse-induced refractive index change is reconstructed from near-field mode profile data using the scalar wave equation and by refractive near-field profiling. Both coarse and fine period gratings are written and characterized, and the thermal stability of these gratings is investigated. The utility of the femtosecond writing technique is demonstrated by fabricating an optical interleaver.

Kro *et al* (2004) reviewed their work on fs-laser fabrication and characterization of photonic structures in glass and discuss the effect of glass composition on processing parameters and structural modification.

Zoubir *et al* (2004), fabricated buried tubular waveguides having an annular core in bulk PMMA by femtosecond laser direct writing. The refractive index profile was obtained from selective etch profiling. Numerical calculation of the propagating modes in the waveguides was performed with a finite-difference method. Good agreement was found between calculation and measurement of the output distribution in the near field.

Cheng (2004) , reported sporadically the surface chemistry modification of PMMA using direct-write laser micromachining to fabricate microfluidic chips. The method developed does not require extensive solvent drying procedures and is therefore simpler and more efficient than existing methods. Organosilane modification largely expands the application of the PMMA as a biochip substrate for that a great variety of surface functional groups can be prepared on the plastic surface with similar procedure. Perfluoroalkylation modification can be used for surface passivation of PMMA to prevent adsorption.

Aminoalkylationand mercaptoalkylation have been used for biomolecule immobilization.

Kazuyoshi (2006), studied the refractive index changes and vacancies that are induced in transparent materials like glass by the irradiation of femtosecond laser pulses. He applied this technique to fabricate three-dimensional photonic structures such as optical data storages, waveguides, gratings, and couplers inside a wide variety of transparent materials. He reported micro-fabrication experiments of optical elements in glasses with femtosecond laser pulses, including fabrication of couplers, Bragg gratings, and zone plates and holograms on the surface of glass. A trial fabrication experiment on organic materials is also reported.

Vishnubhatla *et al* (2008), fabricated micro gratings in silicate, Foturan and tellurite glasses using femtosecond direct writing. Refractive index change in these structures was estimated using optical diffraction technique and was found to be in the order of 10^{-3} sufficient for wave guiding applications. The ability to create such structures, both passive and active, has strong implications in the field of micro-photonic and microfluidic devices.

A. Taranu *et al* (2010), demonstrated the Spatial mapping of photo-chemical and optical density changes in polymethyl methacrylate formed by direct femtosecond laser writing of photonic structures at 180 fs, 387nm and 44fs, 800 nm at 1kHz repetition rate. Their Results show the variations in the monomer content and intensity of background scattering light in the substructure. They noted that this technique needs further refinement but these initial results indicate that it is useful for polymer optical fibres (POF) because it enables the photo-chemical and optical density composition of subsurface photonic structures to be estimated non invasively and refractive index to be estimated.

Bauma *et al* (2011) reported on the fabrication of optical Bragg type phase gratings in polymethyl methacrylate substrates by a femptosecond Ti: Sapphire laser. As for their optical characterization, a spatially resolved microscopy interferometric technique is used to investigate the two-dimensional distribution of the refractive index change produced by the irradiation process. The results suggest that efficient modification of the material can be accomplished for a regime of repeated pulses with long pulses, 250 fs with low laser fluency.

Deepak *et al* (2011) investigated femtosecond-laser-induced microstructures (on the surface and within the bulk), gratings, and craters in four different polymers: polymethyl methacrylate, polydimethylsiloxane, polystyrene, and polyvinyl alcohol. Local chemical modifications leading to the formation of optical centers and peroxide radicals were studied using ultraviolet-visible absorption and emission, confocal micro-Raman and electron spin resonance spectroscopic techniques. Potential applications of these structures in microfluidics, waveguides, and memory-based devices are demonstrated.

A. Baum et al (2011) reported on fabrication of optical Bragg type phase gratings in polymethyl methacrylate substrates by a femptosecond Ti: Sapphire laser. As for their optical characterization, a spatially resolved microscopy interferometric technique is used to investigate the two-dimensional distribution of the refractive index change produced by the irradiation process. The technique gives a direct and quantitative two-dimensional profile of the index of refraction in irradiated PMMA, providing information on how the fabrication process depends on the laser irradiation.

Taleb *et al* (2011), investigated and demonstrated the experimental evidence of the effect of femtosecond laser pulses on the spectral response of a Silicon photovoltaic cell. The observed enhancement is related to the appearing of nano-structured groves in the 700-900 nm range. The responsivity and the conversion efficiency of the photovoltaic cell are enhanced by this technique.

Ultrashort laser pulses should be still economically reasonable in a large scale production.

Oliveira *et al* (2012) reported on a simple method to obtain surface gratings using a Michelson interferometer and femtosecond laser radiation. In the optical setup used, two parallel laser beams are generated using a beam splitter and then focused using the same focusing lens. An interference pattern is created in the focal plane of the focusing lens, which can be used to pattern the surface of materials. The main advantage of this method is that the optical paths difference of the interfering beams is independent of the distance between the beams. The potential of the method was demonstrated by patterning surface gratings with different periods on titanium surfaces in air.

Horn *et al* (2012) reported the fabrication of femtosecond laser-induced, first-order waveguide Bragg gratings in lithium niobate in the low repetition rate regime. Type-II waveguides are written into an x-cut lithium niobate wafer and structured periodically to achieve narrowband reflections at wavelengths around 1550 nm. Additionally, electrodes are employed to allow for electro-optic tuning of the spectral response. And demonstrate wavelength control of the central reflection peak by applying a static external electric field. A maximum shift of the reflection peak of $\Delta\lambda=625$ pm is observed.

Buividas *et al* (2012) reported in high-precision surface ablation, film removal, ripple formation are presented. They discussed volume processing via polymerization, marking, dicing, cutting, and drilling of semiconductor and dielectric materials. And focused on processes which can be carried out at a high throughput in the industrial environment or/and can deliver functionalities currently not amenable by competing technologies. Unique features of direct laser writing by femtosecond laser pulses are highlighted. Methodology for solutions of engineering tasks is presented. Namely, the laser irradiation

parameters are selected on the basis of the required processing conditions for the material of a work-piece.

Deepak *et al* (2012) investigated femtosecond-laser-induced microstructures (on the surface and within the bulk), gratings, and craters in four different polymers: polymethyl methacrylate, polydimethylsiloxane, polystyrene, and polyvinyl alcohol. Local chemical modifications leading to the formation of optical centers and peroxide radicals were studied using ultraviolet-visible absorption and emission, confocal micro-Raman and electron spin resonance spectroscopic techniques. Potential applications of these structures in microfluidics, waveguides, and memory-based devices are demonstrated.

1.3. Objectives:

This work aimed mainly to:

- Fabricating of photonic structures sub surface in Polymethylmethacrylate (PMMA) by means of Coherent Legend Ti: Sapphire laser facility generated horizontal linear polarized light, pulsed at a 1-kHz repetition rate, with pulse duration of 250 fs laser at a central wavelength of about 800 nm. The output beam from the system had laser pulse energy of 0.105 µJ in the Gaussian mode with a diameter of ~3mm.
- Characterization of the induced sub surface texturing by means of Interference technique and matlab programme.
- Track the variations that happen due to the modification of PMMA sample.

1.4. Thesis layout:

The thesis comprises of four chapters; chapter one contains a short introduction to surface modification, Refractive Index, Interferometry, and previous studies. Chapter two involves a detailed theoretical background and basic concepts of Interference, Characterization of Polymethylmethacrylate (PMMA), Laser Direct Writing (LDW) Processing, and Laser Material Interaction The experimental part is fully described and presented in chapter three. Then the results had been presented, analyzed and discussed in chapter four and finally a short conclusion of this research and recommendations were presented and followed by a list of References and Appendex.

Chapter Two

Theoretical background

2.1. The differential equation of light rays

The light rays have been defined as the orthogonal trajectories to the geometrical wave-fronts S(x, y, z) = constant and we have seen that, if **r** is a position vector of a typical point on a ray and s the length of the ray measured from a fixed point on it, then

$$n\frac{d\mathbf{r}}{ds} = \text{grad } \mathcal{S}.$$

(2.1)

This equation specifies the rays by means of the function S, but one can easily derive from it a differential equation which specifies the rays directly in terms of the refractive index function n(r).

Differentiating $(2,1)$ with respect to s we obtain

$$\frac{d}{ds}\left(n\frac{dr}{dn}\right) = \frac{d}{ds}(grad\ S)$$

$$= \frac{d}{ds} \cdot grad\ (grad\ S)$$

$$= \frac{1}{n}\ grad\ S \cdot grad\ (grad\ S) \qquad (\text{ by } (2.1))$$

$$= \frac{1}{2n}\ grad\ \left[(grad\ S)^2\right]$$

$$= \frac{1}{2n}\ grad\ n^2 \qquad \text{from} \qquad (\text{grad}\,\mathcal{S})^2 = n^2,$$

i.e.

$$\frac{d}{ds}\left(n\frac{d\mathbf{r}}{ds}\right) = \text{grad } n. \tag{2.2}$$

This is the vector form of the differential equations of the light rays. In particular, in a homogeneous medium n = constant and (2.2) then reduces to

$$\frac{d^2 r}{d s^2} = 0.$$

whence

$$r = s\mathbf{a} + \mathbf{b}, \tag{2.3}$$

a and **b** being constant vectors. Eq. (2.3) is a vector equation of a straight line in the direction of the vector **a**, passing through the point **r** = **b**. Hence in a homogeneous medium the light rays have the form of straight lines.

As an example of some interest, let us consider rays in a medium which has spherical symmetry, i.e. where the refractive index depends only on the distance r from a fixed point O:

$$n = n(r). \tag{2.4}$$

This case is approximately realized by the earth's atmosphere, when the curvature of the earth is taken into account.

Consider the variation of the vector $\mathbf{r} \times [n(r)\, s]$ along the ray. We have

$$\frac{d}{ds}(\mathbf{r} \times n\mathbf{s}) = \frac{d\mathbf{r}}{ds} \times n\mathbf{s} + \mathbf{r} \times \frac{d}{ds}(n\mathbf{s}). \tag{2.5}$$

Since dr/ds = s, the first term on the right vanishes. The second term may, on account of (2.2), be written as $\mathbf{r} \times \text{grad } n$. Now from (2.4)

$$grad\ n = \frac{r\,d\,n}{r\,d\,r}\ ,$$

so that the second term on the right-hand side of eq. (2.5) also vanishes. Hence

$$\mathbf{r} \times n\mathbf{s} = \text{constant}. \tag{2.6}$$

This relation implies that all the rays are plane curves, situated in a plane through the origin, and that along each ray

$$nr \sin \phi = \text{constant}, \tag{2.7}$$

where ø is the angle between the position vector $\mathbf{r}$ and the tangent at the point $\mathbf{r}$ on the ray (see Fig. 2.1). Since $\mathbf{r}$ sin ø represents the perpendicular distance d from the origin to the tangent, eq. (2.7) may also be written as

$$nd = \text{constant}. \tag{2.8}$$

This relation is sometimes called the formula of Bouguer and analogue of a well-known formula in dynamics, which expresses the conservation of angular momentum of a particle moving under the action of a central force.

To obtain an explicit expression for the rays in a spherically symmetrical medium,

We recall from elementary geometry that, if (r,θ) are the polar coordinates of a plane.
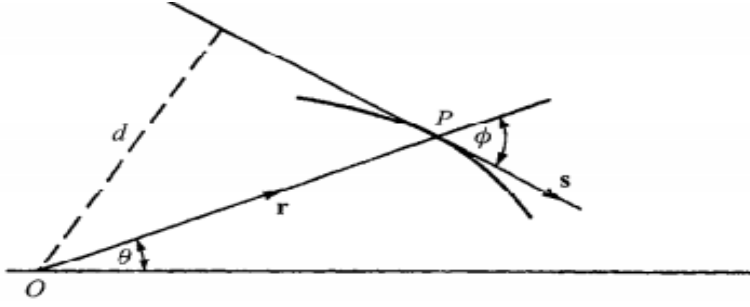
Figuure 2.1 Illustrating Bouguer's formula nd = constant, for rays in a medium with spherical symmetry.

curve, then the angle ø between the radius vector to point P on the curve and the tangent at P is given by

$$\sin \phi = \frac{r(\theta)}{\sqrt{r^2(\theta) + \left(\frac{dr}{d\theta}\right)^2}}.$$

(2.9)

From eq. (2.7) and eq. (2.9)

$$\frac{dr}{d\theta} = \frac{r}{c}\sqrt{n^2 r^2 - c^2},$$

(2.10)

c being a constant. The equation of rays in a medium with spherical symmetry may therefore be written in the form

$$\theta = c \int^r \frac{dr}{r\sqrt{n^2 r^2 - c^2}}.$$

(2.11)

Let us now return to the general case and consider the curvature vector of a ray, i.e. the vector

$$K = \frac{ds}{ds} = \frac{1}{\rho}v$$

(2.12)

Whose magnitude 1/ρ is the reciprocal of the radius of curvature, v is the unit principal normal at a typical point of the ray.

16

From eq. (2.2) and eq. (2.12) it follows that

$$nK = \operatorname{grad} n - \frac{dn}{ds}\mathbf{s}.$$

(2.13)

This relation shows that the gradient of the refractive index lies in the osculating plane of the ray.

If we multiply eq. (2.13) scalarly by K and use eq. (2.12) we find that

$$|\mathbf{K}| = \frac{1}{\rho} = \mathbf{v} \cdot \operatorname{grad} \ln n.$$

(2.14)

(Courant R. 1942)
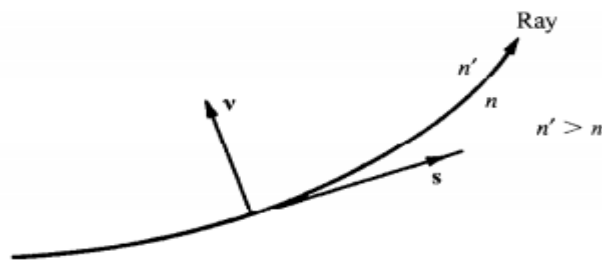
Figure 2.2 Bending a ray in a heterogeneous medium.
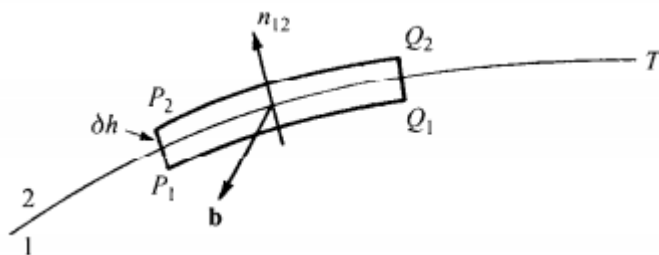
Figure 2.3 Illustration of the laws of refraction and reflection.

Since ρ is always positive, this implies that as we proceed along the principal normal the refractive index increases, i.e. the ray bends towards the region of higher refractive index (Fig. 2.2).[Max Born and Wolf (2003)]

2.2. Plane Wave:

The simplest example of an electromagnetic wave is the plane wave. The plane wave is produced by a monochromatic point source at infinity and is approximated by a collimated light source. The complex amplitude of a linearly polarized plane wave is

$$\mathbf{E}(x, y, z, t) = \mathbf{E}(\mathbf{r}, t) = \mathbf{A}e^{i[\omega t - \mathbf{k} \cdot \mathbf{r}]} \tag{2.15}$$

Where k is the wave vector. The wave vector points in the direction of propagation, and its magnitude is the wave number $k = 2\pi / \lambda$, where λ is the wavelength.

2. 3. Spherical Wave:

The second special case of an electromagnetic wave is the spherical wave which radiates from an isotropic point source. If the source is located at the origin, the complex amplitude is

$$E(r, t) = (A/r)e^{i[\omega t - kr]} \tag{2.16}$$

Where $r = (x^2 + y^2 + z^2)^{1/2}.$
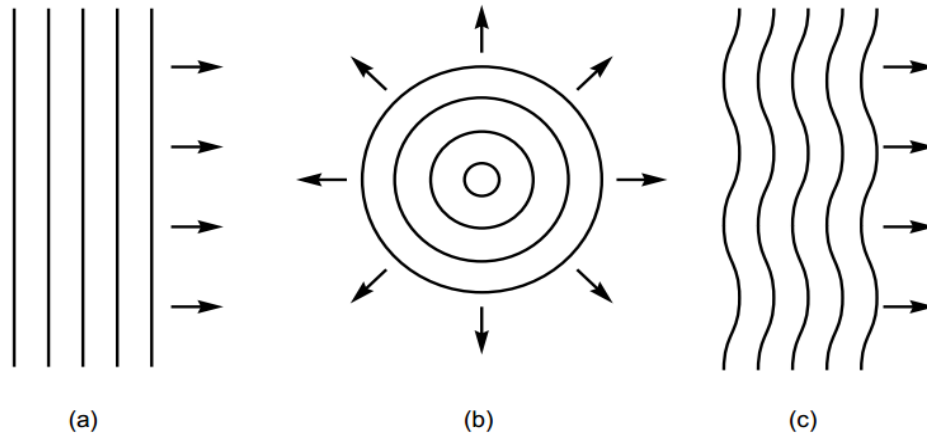
Figure 2.4. Examples of wavefronts : (a) plane wave ; (b) spherical wave ; and (c) aberrated plane wave.

2. 4. Wavefronts:

Wavefronts represent surfaces of constant phase for the electromagnetic field. Since they are normally used to show the spatial variations of the field, they are drawn or computed at a fixed time. Wavefronts for plane and spherical waves are shown in Fig. 1a and b. The field is periodic, and a given value of phase will result in multiple surfaces. These surfaces are separated by the wavelength. A given wavefront also represents a surface of constant optical path length (OPL) from the source. The OPL is defined by the following path integral:

$$OPL = \int_S^P n(s)\, ds$$

(2.17)

Where the integral goes from the source S to the observation point P, and n(s) is the index of refraction along the path. Variations in the index or path can result in irregularities or aberrations in the wavefront. An aberrated plane wavefront is shown in Fig. 1c. Note that the wavefronts are still separated by the wavelength.

The local normal to the wavefront defines the propagation direction of the field. This fact provides the connection between wave optics and ray or geometrical optics. For a given wavefront, a set of rays can be defined using the local surface normals. In a similar manner, a set of rays can be used to construct the equivalent wavefront.

2.5. Interference:

Interference results from the superposition of two or more electromagnetic waves. From a classical optics perspective, interference is the mechanism by which light interacts with light. Other phenomena, such as refraction, scattering, and dif fraction, describe how light interacts with its physical environment. Historically, interference was instrumental in establishing the wave nature of light. The earliest observations were of colored fringe patterns in thin films. Using the wavelength of light as a scale, interference continues to be of great practical importance in areas such as spectroscopy and metrology.

The net complex amplitude is the sum of all of the component fields,

$$\mathbf{E}(x, y, z, t) = \sum_i \mathbf{E}_i(x, y, z, t)$$

(2.18)

And the resulting field intensity is the time average of the modulus squared of the total complex amplitude

$$I(x, y, z, t) = \langle |\mathbf{E}(x, y, z, t)|^2 \rangle$$

(2.19)

Where $\langle \ \rangle$ indicates a time average over a period much longer than $1/\nu$. If we restrict ourselves to two interfering waves E 1 and E 2, this result simplifies to

$$I(x, y, z, t) = I_1 + I_2 + \langle \mathbf{E}_1 \cdot \mathbf{E}_2^* \rangle + \langle \mathbf{E}_1^* \cdot \mathbf{E}_2 \rangle$$

(2.20)

Where I1 and I2 are the intensities due to the two beams individually, and the (x, y, z, t) dependence is now implied for the various terms.

2.5.1. Interference Fringes:

We will now add the additional restrictions that the two linear polarizations are parallel and that the two waves are at the same optical frequency. The expression for the intensity pattern now becomes

$$I(x, y, z) = I_1 + I_2 + 2\sqrt{I_1 I_2} \cos \left[\Delta\phi(x, y, z) \right] \qquad (2.21)$$

Where $\Delta\phi = \phi_1 - \phi_2$ is the phase difference. This is the basic equation describing interference. The detected intensity varies cosinusoidally with the phase difference between the two waves as shown in Fig. 2.5
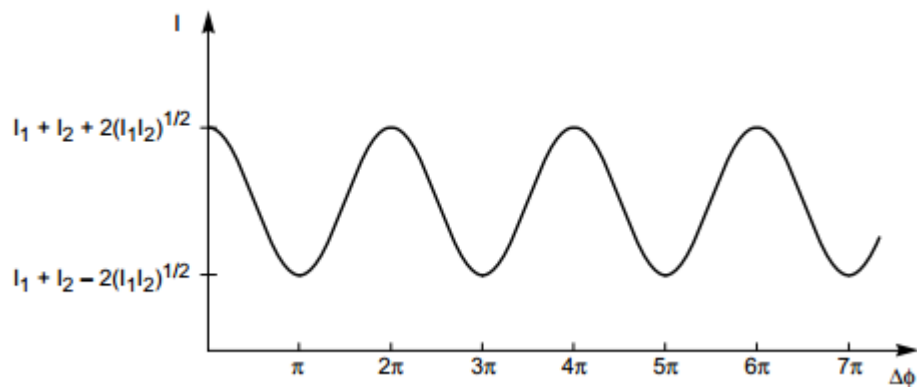

Figure 2.5 The variation in intensity as a function of the phase difference between two interfering waves.

These alternating bright and dark bands in the intensity pattern are referred to as interference fringes, and along a particular fringe, the phase difference is constant.

Table 2.1 The Phase Dif ference and OPD for

Bright and Dark Fringes (m an Integer)

	$\Delta\phi$	OPD
Bright fringe	$2m\pi$	$m\lambda$
Dark fringe	$2(m+1)\pi$	$(m+1/2)\lambda$

The phase difference is related to the difference in the optical path lengths between the source and the observation point for the two waves. This is the optical path difference (OPD):

$$OPD = OPL_1 - OPL_2 = \left(\frac{\lambda}{2\pi}\right)\Delta\phi$$

$$\Delta\phi = \left(\frac{2\pi}{\lambda}\right)OPD \tag{2.22}$$

1- The phase difference changes by 2π every time the OPD increases by a wavelength. The OPD is therefore constant along a fringe. Constructive interference occurs when the two waves are in phase, and a bright fringe or maximum in the intensity pattern results. This corresponds to a phase difference of an integral number of 2π's or an OPD that is a multiple of the wavelength. A dark fringe or minimum in the intensity pattern results from destructive interference when the two waves are out of phase by π or the OPD is an odd number of half wavelengths. These results are summarized in Table 1.For conditions between these values, an intermediate value of the intensity results. Since both the OPD and the phase difference increase with the integer m, the absolute value of m is called the order of interference.   As we move from one bright fringe to an adjacent bright fringe, the phase difference changes by 2π. Each fringe

period corresponds to a change in the OPD of a single wavelength. It is this inherent precision that makes interferometry such a valuable metrology tool. The wavelength of light is used as the unit of measurement. Interferometers can be configured to measure small variations in distance, index, or wavelength.

When two monochromatic waves are interfered, the interference fringes exist not only in the plane of observation, but throughout all space. This can easily be seen from Eq. (2.21) where the phase difference can be evaluated at any z position. In many cases, the observation of interference is confined to a plane, and this plane is usually assumed to be perpendicular to the z axis. The z   dependence in Eq. (2.21) is therefore often not stated explicitly, but it is important to remember that interference effects will exist in other planes. [M. Bass, et al *, (1995).*].

2.5.2. The Mach–Zehnder interferometer :

In the Jamin interferometer the front surfaces of the two plates act as beam-dividers and the rear surfaces as plant mirrors, but these elements cannot be adjusted independently, and the separation of the two beams is limited by the thickness of the plates. A much more versatile instrument. In which the beams may be widely separated, is obtained when the beam-dividers and mirrors the separate elements. This is the basis of the. Mach-Zehnder interferometer, which is used to measure variations of refractive index, and hence of density, in compressible gas flows.

The arrangement is shown in Fig.2.6. Light from a source S in the focal plane of a well-corrected lens L_1 is divided at the semireflecting surface A_1 of a plane-parallel glass plate D_1 into two beams, which, after reflection at plane mirrors M_1, M_2, are recombined at the semireflecting surface A_2 of a second identical plane-parallel plate D_2, and emerge to a

well-corrected collecting lens L_2. The four reflecting surfaces are usually arranged to be approximately parallel, with their centres at the corners of a parallelogram. Suppose the source is a point source of quasi-monochromatic light. Let W_1 be a plane wave-front in the beam between M_1 and D_2, W_2 the corresponding plane wave-front in the beam between M_2 and D_2 and W the virtual plane wave-front between M_2 and D_2 which would emerge from D_2 coincident and cophasal with W_1. At point P on W_2 the virtual phase difference between the emergent beams is then

$$\delta = \frac{2\pi}{\lambda_0} nh,$$
(2.23)

where $h = PN$ is the normal distance from P to $W`_1$, and n is the refractive index of the medium between $W_2$ and $W`_1$. At the point $P`$ in the emergent beams, conjugate to P, there will be a bright fringe if

$$nh - m\lambda_0, \qquad |m| = 0, 1, 2, \ldots,$$
(2.24a)

and a dark fringe if

$$nh = m\lambda_0, \qquad |m| = \tfrac{1}{2}, \tfrac{3}{2}, \tfrac{5}{2}, \ldots.$$
(2.24b)

When $W`_1$ and W_2 are parallel, the intensity is the same for all P, and under these circumstances an extended source would give fringes at infinity (i.e. in the focal plane of L_2) similar to those of the Jamin interferometer.
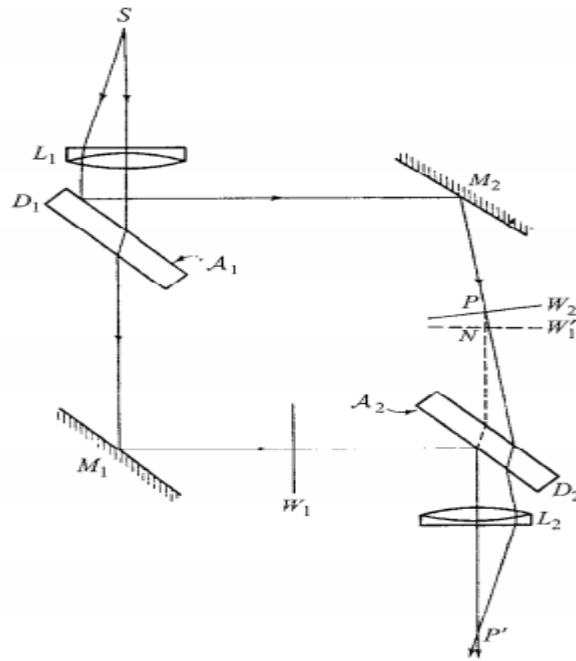
Figure 2.6 the Mach-zehnder interferometer.

In general, however, $W`_1$ and W_2 are mutually inclined, and the fringes are straight lines parallel to their intersection. It is these wedge fringes that are normally used in the examination of gas flows, and because of intensity considerations it is desirable to form them with the largest source extension possible without loss of visibility. The fringes then become localized in the region where intersecting rays have the smallest angular separation on leaving S. The position of this region of localization can be varied by varying the combination of rotations of the elements used to produce the mutual inclination of $W`_1$ and W_2. For example, if the reflecting surfaces are initially parallel, and if for simplicity we consider the case of rotations about axes perpendicular to the plane of centres, the virtual region of localization is near M_2 when M_2 is rotated [Fig. 2.7 (a)], but lies between M_2 and D_2 when both M_2 and D_2 are rotated [Fig. 2.7 (b)]. This property distinguishes the wedge fringes of the Mach-Zehnder interferometer from those given by the Michelson

interferometer with collimated light which are virtually localized in the vicinity of the mirrors.
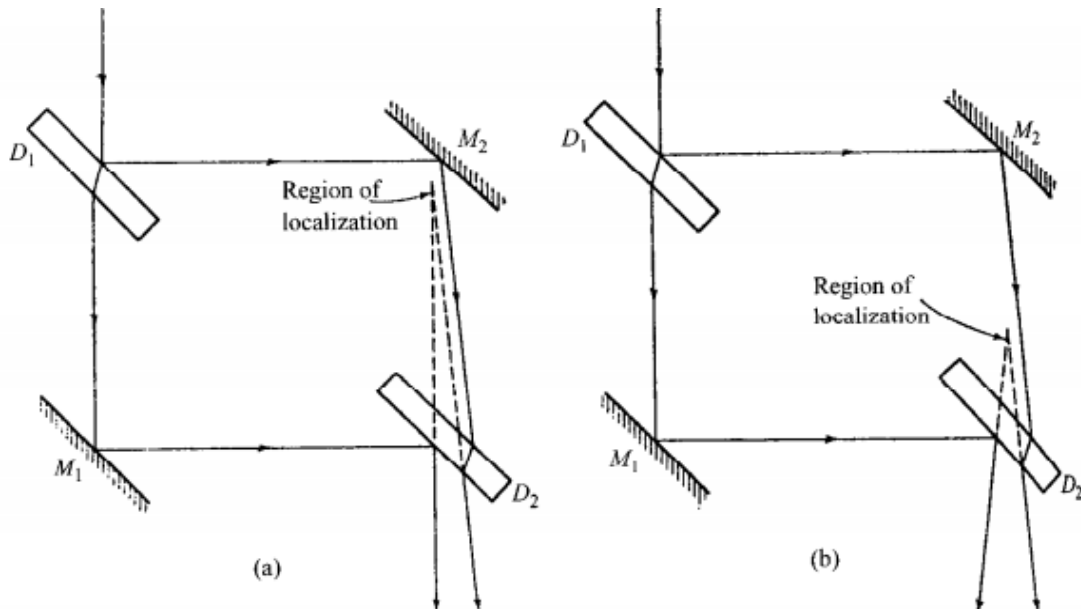
Figure 2.7: Illustrating fringe localization in the Mach-Zehnder interfererometer.

2.6. Types of grating:

The principle of the diffraction grating was discovered by Rittenhouse in 1785, but this discovery attracted practically no attention. The principle was re-discovered by fraunhofer in 1891. fraunhofer's first grating were made by winding very fine wire round two parallel screws. Because of the relative ease with which wire grating may be constructed these are occasionally used even today, particularly in the long-wavelength (infra-red) range. Later fraunhofer made gratings with the help of a machine, by ruling through gold films deposited on a glass plate, also, using a diamond as a ruling point, he ruled the grooves directly onto the surface of glass. [Harrison G. R., (1949)].

Great advances in the technique of production of grating were made by Rowland who constructed several excellent ruling machines and also invented the so-called concave grating. Rowland's machine was able to rule gratings with grooves over 4 in long over a length of 6 in, and his first machine ruled about 14,000 grooves per inch, giving a resolving power in excess of 150,000. Later Michelson ruled gratings considerably wider than 6 in, with a resolving power approaching 400,000.

Most of the early gratings were ruled on speculum metal and glass, but the more recent practice is to rule the grooves on evaporated layers of aluminium. Since aluminium is a soft metal it causes less wear on the ruling point (diamond) and it also reflects better in the ultra-violet.

A perfect grating would have all the grooves strictly parallel and of identical form, but in practice errors will naturally occur. Quite irregular errors lead to a blurring of the spectrum and are not so serious as systematic errors, such as periodic errors of spacing. These errors give rise to spurious lines in the spectrum, known as ghosts. Often they can be distinguished from true lines only with difficulty. High resolving power is not always the only important requirement in spectroscopic applications. When little energy is available, as for example in the study of spectra of faint stars or nebulae, or for work in the infra-red region of the spectrum, it is essential that as much light as possible should be diffracted into one particular order. Moreover, for precise wavelength measurements, a grating that gives high dispersion must be used. According to

$$p \equiv \sin\theta - \sin\theta_0 = \frac{m\lambda}{d} \qquad (m = 0, \pm 1, \pm 2, \ldots).$$

the angular dispersion (with a fixed angle of incidence) is given by

$$\frac{\mathrm{d}\theta}{\mathrm{d}\lambda} = \frac{1}{\cos\theta}\frac{m}{d},$$

(2.25)

So that to obtain high dispersion the spacing d should be small or the observations must be made in high orders (m large). If, however, the grating is formed by a succession of opaque and transparent (or reflecting) strips, only a small fraction of the incident light is thrown into any one order. This drawback is overcome in modern practice by ruling the grooves to controlled shape. With a grating which consists of grooves of the form shown in Fig. 2.8, most of the light may be directed into one or two orders on one side of the central image. Grating of this type, with fairly coarse grooves, are called echelette gratings, because they may be regarded as being intermediate between the older types of grating and the so-called echelon gratings which will be described later. Echlette grating were first ruled by Wood on copper
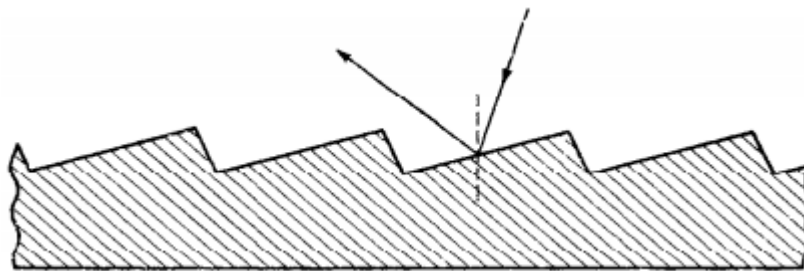
Figure 2.8: Reflection grating with controlled groove form.

Plates, using the natural edge of a selected carborundum crystal as ruling point. Later they were ruled with diamond edges ground to the desired shape. They had 2000 – 3000 grooves per inch, and when used with visible light they sent the greater part of the light into a group of spectra near the 15th or 30th order. Echelette gratings have considerable value in infra-red spectroscopy.

More recently have been developed for controlling the groove shape for gratings with must smaller groove spacing. [R. W. Wood, (1937), H Babcock, (1944)], These blazed gratings, as they are called, have grooves of similar form as the echelettes. But form the most intense spectra in muchlwer orders (usually the first or second).

It appears that the resolving power of grating of the type described is limited by practical considerations of manufacture to about 400,000. For some applications (e.g. for the study of Zeeman effects and the hyperfine and isotope structure patterns), a resolving power that exceeds this value is required. For the attainment of such a high resolving power, Harrison [G. R. Harrison, (1949)].

proposed the so-called echelle grating, which has wide, shallow grooves and is designed for use at an angle of incidence greater than 45°, the direction of incidence being normal to the narrow side of the step. These gratings operate with relatively high orders (m ~ 1000). A 10 in echelle with 100 grooves per inch, designed for observation in the 1000th order, has a resolving power of 1,000,000.

Because a grating of good quality is very difficult to produce, replicas of original rulings are often used . These are obtained moulding from an original ruled master grating.

Finally we must mention a grating of an entirely different construction, the echelon invented by Michelson [A. A. Michelson, (1898).]. It consists of a series of strictly similar plane-parallel glass plates arranged in the form of a flight of steps (hence the name), as shown in Fig. 2.9 Each step retards the beam of light which passes through it by the same amount with respect to its neighbour. Because the breadth of each step is large compared to the wavelength, the effect of diffraction is confined to small

angles, so that most of the light is concentrated in one or two spectra near the direction $\theta = 0$, and these correspond to very high orders, since the retardation introduced between successive beams is very many wavelengths.

The resolving power of the echelon depends not only on the path difference between the rays from the extreme ends of the grating but also (through to a much lesser extent) on the dispersion of the glass. If n is the refractive index, t the thickness of each step, and d its breadth (see Fig.2.9), the path difference between rays diffracted from neighbouring steps is evidently pd + (n – 1) t, it being assumed p is small. Hence the positions of the principal maxima are given by

$$pd + (n - 1)t = m\lambda, \qquad (m = 0, 1, 2, \ldots).$$

(2.26)

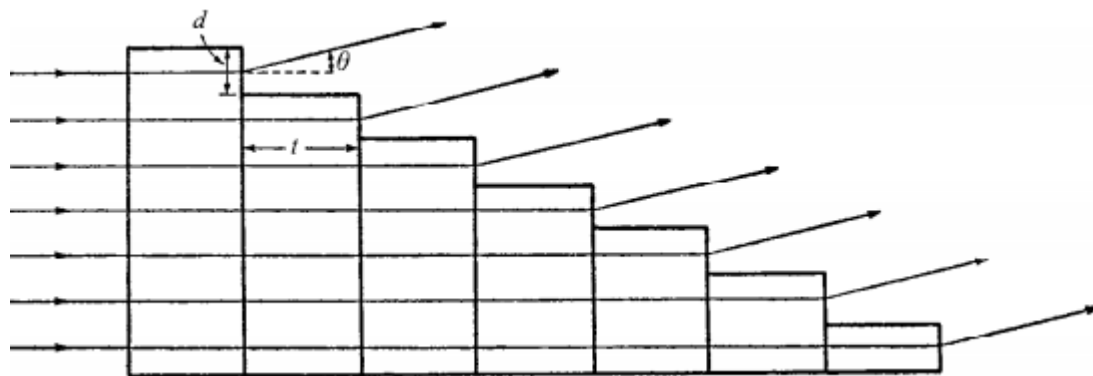Figure 2.9 Michelson's echelon.

If the wavelength is changed by an amount $\Delta\lambda$, the mth-order maximum is displaced by

$$\Delta'p = \left| m - t\frac{dn}{d\lambda} \right| \frac{\Delta\lambda}{d}.$$

(2.27)

The separation Δp between a principal maximum of order m and a neighbouring minimum is again given by $\Delta p = \frac{\lambda}{Nd}$, so that the condition $\Delta p = \Delta' p$ for the limit of resolution gives

$$\frac{\lambda}{\Delta\lambda} = N \left| m - \frac{dn}{d\lambda} t \right|.$$
(2.28)

Here we may substitute for m the value (n − 1) t/λ obtained from (2.26) by neglecting the term pd, for the p values for which the intensity is appreciable are of the order of λ/d, i.e. pd is of the order of a wavelength, whilst (n − 1) t is of the order of many thousand wavelengths. We thus obtain the following expression for the resolving power of the echelon:

$$\frac{\lambda}{\Delta\lambda} \sim N \left| \frac{n-1}{\lambda} - \frac{dn}{d\lambda} \right| t.$$
(2.29)

The ratio $(dn/d\lambda)/[(n-1)/\lambda]$ is small. For flint glass near the centre of the visible region it has a value near − 0.05 to − 0.1. Hence under these circumstances, the resolving power of an echelon exceeds, by about 5 − 10 per cent, the resolving power a line grating with N grooves, when observation is made in the order m = (n − 1) t/λ. One of Michelson's echelone consisted of twenty plates, each having a thickness   t = 18 mm, and the breadth d of each step was about 1 mm. Taking n = 1.5, the retardation between two successive beams measured in wavelengths of green light $\lambda = 5 \times 10^{-5}$ cm was $m \sim 0.5 \times 1.8 / 5 \times 10^{-5} \sim 20,000$. Assuming $(dn/d\lambda)/[(n-1)/\lambda] = -0.1$, this gives a resolving power of about 20 (20,000 + 0.1 × 20.000) = 440, 000.

More important is the reflection echelon. Here each step is made highly reflecting by means of metallic coating, and the spectra formed by reflected light are observed. With a reflection echelon of the resolving

power is 3 – 4 times larger than with a transmission echelon of corresponding dimensions, since each step introduces a retardation between successive beams of amount 2 t instead of (n – 1) t ~ t/2. Like the echelle grating the reflection echelon is capable of giving resolving power of over one million. Another advantage of the reflection echelon over the transmission echelon is that it may be used in the ultra-violet region of the spectrum, where glass absorbs. Although Michelson realized that advantage would be gained by using the instrument with reflected rather than transmitted light, technical difficulties prevented the production of a satisfactory reflection echelon for nearly thirty years unit were overcome by Williams. *Because of difficulties in assembling a large number of plates of equal thickness within the narrow permissible tolerance, the number of steps is limited in practice to about forty.

Finally, a few remark must be made about overlapping of orders Restricting ourselves to the visible region, i.e. considering wavelength in the ranger $\lambda_1 = 0.4$ μm to $\lambda_2 = 0.75$ μm, we see that the first order spectrum dose not quite reach to the spectrum of the second order, for the first order spectrum covers the range from $p = \lambda_1/d$ to $p = \lambda_2/d = 0.75\lambda_1/0.4d = 1.8\lambda_1/d$ whilst the second order begins at $p = 2\lambda_1/d$. On the other hand the spectrum of the second order extends across a part of the third order spectrum, namely from $p = 2\lambda_1/d$ to $p = \lambda_2/d$ whilst the third order begins already at $2 \times 1.8\ \lambda1/d$. As the order increases the successive spectra overlap more and more. If the lines of wavelength λ and $\lambda + \delta\lambda$ coincide in two successive order (m + 1)th and mth, than

$$(m + 1)\lambda = m(\lambda + \delta\lambda)$$

i.e.
$$\frac{\delta\lambda}{\lambda} = \frac{1}{m}.$$
(2.30)

Thus the free spectral range is inversely proportional to the order.

The overlapping of orders was formerly used to compare wavelengths, in the so-called method of coincidences, this has been superseded by simple interpolation between standard wavelengths determined interferometrically.

In conclusion let us summarize the main distinguishing features of the different types of gratings. We recall that, according to (2.14), high resolving power may be attained.
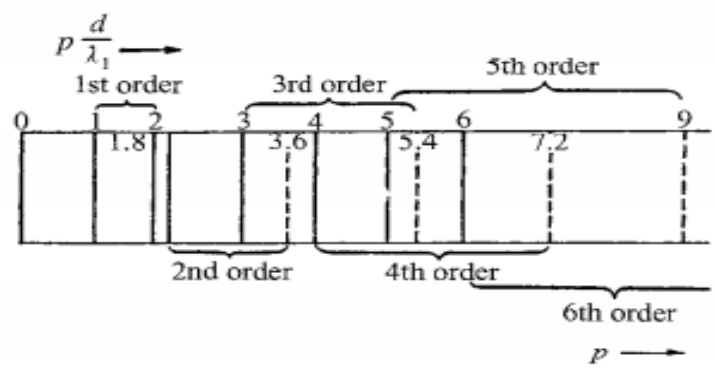
Figure 2.10 The overlapping of grating spectra

with either a large number of periods and relatively low orders, or with a moderate number of periods and large orders. Ordinary ruled grating represent the low-order extreme (m ~ 1 to 5), whilst the echelons represent the extreme of high order (m ~ 1000). For particular applications one must bear in mind that the angular dispersion is directly proportional to the spectral order and inversely proportional to the period whilst the free spectral range is inversely proportional to the order.

[Max Born and Wolf.(2003)] .

2.7. Poly (methyl methacrylate) (PMMA):

Properties of special interest: optically clear (92% transmission, theoretical limit for normal incidence, in the visible region) through the wavelength range; very little ultraviolet absorption until 260nm. Good medical properties. Extremely high weather ability. Replacement for glass. Can be used as one-component-deep UV, electron-beam, or ion – beam resists in the manufacture of microelectronics chips, [Thompson, et al, (1984). Htoo, M. S., (1989)].

It is high sensitivity to electron radiation at an electron-beam energy of 25kev and main chain scission ($0.5Jcm^{-2}$ at 26kev) and UVmain chain scission of about (4-6ev, $0.6Jcm^{-2}$) [Clough, R. L., and S. W. Shalaby (1991)].

The most important member of the acrylic polymers is poly(methyl methacrylate). It is a hard, clear, colorless, transparent plastic that is usually available as molding and extrusion pellets, reactive syrups, cast sheets, rods, and tubes.

Poly (methyl methacrylate) for molding or extrusion is produced commercially by free-radical-initiated suspension or bulk polymerization of methyl methacrylate. To minimize polymerization reaction exotherm and shrinkage, bulk polymerization, which is used in the production of sheets, rods and tubes, is carried out with a reactive syrup of partially polymerized methyl methacrylate, which has a viscosity convenient for handling. Poly(methyl methacrylate) is an amorphous polymer composed of linear chains. The bulky nature of the pendant group (–O–CO–Me), and the absence of complete stereo regularity makes PMMA an amorphous polymer. Isotactic and syndiotactic PMMA may be produced by anionic polymerization of methyl methacrylate at low temperatures.

However, these forms of PMMA are not available commercially. Modified PMMA can be obtained by copolymerizing methyl methacrylate with monomers such as acrylates, acrylonitrile, and butadiene. Poly(methyl methacrylate) is characterized by crystal-clear light transparency, unexcelled weather ability, and good chemical resistance and electrical and thermal properties. It has a useful combination of stiffness, density, and moderate toughness. PMMA has a moderate T gof 105°C, a heat deflection temperature in the range of 74 to 100°C, and a service temperature of about 93°C. However, on pyrolysis, it is almost completely depolymerized to its monomer. The outstanding optical properties of PMMA combined with its excellent environmental resistance recommend it for applications requiring light transmission and outdoor exposure.

Polymethyl methacrylate (PMMA), a clear plastic, is a pretty versatile material. Plexiglas windows are made from PMMA. Acrylic paints contain PMMA. It also remains one of the most enduring materials in orthopedic surgery where it has a central role in the success of total joint replacement. Being part of a group of medical materials called 'bone cement', its use includes the fixation of biomaterials such as artificial joints to bone, the filling of bone defects and, also, as a drug-delivery system[Manoj et al (2012)]. Poly (methacrylates) are polymers of the esters of methacrylic acids. The most commonly used among them is poly (methyl methacrylate) (PMMA). Poly (methyl methacrylate) or poly (methyl 2-methylpropenoate) is the polymer of methyl methacrylate, with chemical formula $(C_5H_8O_2)_n$. It is a clear, colourless polymer available on the market in both pellet and sheet form under the names Plexiglas, Acrylite, Perspex, Plazcryl, Acrylplast, Altuglas, Lucite etc. It is commonly called acrylic glass or simply acrylic. Another

polymer, poly(methyl acrylate) (PMA) is a rubbery material, similar to poly(methyl methacrylate), but softer than it, because its long polymer chains are thinner and smoother and can more easily slide past each other.

2.7.1. Structure

Poly(methyl methacrylate) is produced by free-radical polymerization of methylmethacrylate in mass (when it is in sheet form) or suspension polymerization according to the following chart:

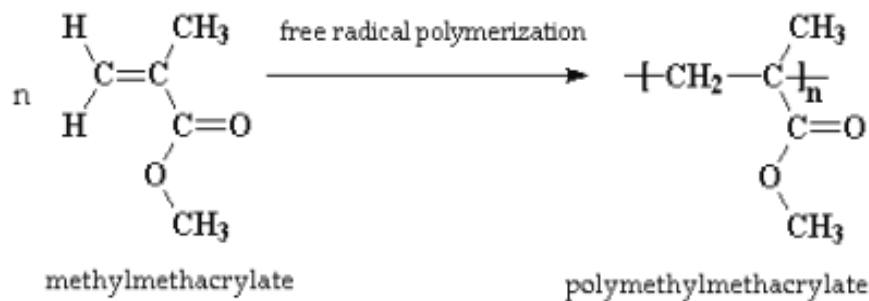Figure 2.11: A chart of free-radical polymerization of methylmethacrylate

2.7.2 Physical and mechanical properties of PMMA:

PMMA is a linear thermoplastic polymer. PMMA has a lack of methyl groups on the backbone carbon chain - its long polymer chains are thinner and smoother and can slide past each other more easily, so the material becomes softer. Main physical characteristics of PMMA are shown in table 2.2.

Table 2.2 Typical physical properties of Polymethyl methacrylate.

Physical Properties	Value
Density	1.15 - 1.19 g/cm3
Water Absorption	0.3 – 2 %
Moisture Absorption at Equilibrium	0.3 - 0.33 %
Linear Mould Shrinkage	0.003 - 0.0065 cm/cm
Melt Flow	0.9 – 27 g/10 min

PMMA has high mechanical strength, high Young's modulus and low elongation at break. It does not shatter on rupture. It is one of the hardest thermoplastics and is also highly scratch resistant. It exhibits low moisture and water absorbing capacity, due to which products made have good dimensional stability. Both of these characteristics increase as the temperature rises. Table 2.3 shows some of mechanical characteristics of PMMA.

Table 2.3 Mechanical characteristics of Polymethyl methacrylate

Mechanical Properties	Value
Hardness, Rockwell M	63 - 97
Tensile Strength, Ultimate	47 - 79 MPa
Elongation at Break	1 - 30 %
Tensile Modulus	2.2 - 3.8 GPa
Flexural Modulus	3 - 3.5 GPa
Izod Impact, Notched	1.2 – 20k J/m
Izod Impact, Unnotched	11kJ/m
Tensile Creep Modulus, 1 h	1800 - 2700 MPa
Tensile Creep Modulus, 1000	h 1200 - 1800 MPa

Its strength properties during injection moulding differ significantly in longitudinal and transverse direction as a result of the orientation effect. As in the case with other thermoplastics, the mechanical properties of PMMA vary as the temperature changes. This material tends to creep. It is not suitable for operation under multiple dynamic loads.

PMMA is one of the polymers that is most resistant to direct sunshine exposure. Its strength characteristics exhibit fairly small variations under the effect of UV-radiation, as well as in the presence of ozone. These properties of PMMA make it suitable for products intended for long open-air operation.

2.7.3 Electrical characteristics of PMMA:

The low water absorption capacity of PMMA makes it very suitable for electrical engineering purposes. Its dielectric properties are very good, but polystyrene and LDPE are superior to it. Its resistivity depends on the ambient temperature and relative humidity. The dielectric constant, as well as the loss tangent, depends on the temperature, the relative humidity of air and the frequency. Table 2.4 shows some of Electrical characteristics of PMMA.

Table 2.4 Electrical properties of Polymethyl methacrylate.

Electrical Properties	Value
Electrical Resistivity	10^{14} - 10^{15} Ω.cm
Surface Resistance	10^{14} - 10^{16} Ω
Loss factor, 20°C, 1000 Hz, 60% humidity	0.04
Dielectric Constant	2.8 - 4
Dielectric Constant, Low Frequency	3 - 4
Dielectric Strength	17.7 - 60 kV/mm
Dissipation Factor	0.03 - 0.55
Arc Resistance	**2** - 180 s

2.7.4 Thermal properties of PMMA:

The thermal stability of standard PMMA is only 65°C. Heat-stabilized types can withstand temperatures of up to 100°C. PMMA can withstand temperatures as low as -70°C. Its resistance to temperature changes is very good.

PMMA is a combustible material, which continues burning even after the flame is removed – the products separated in the process of thermal destruction have an intoxicating effect.

Table 2.5 Thermal properties of Poly (methyl methacrylate)

Thermal Properties	Value
CTE, linear 20°C	60 - 130 μm/m.°C
CTE, linear 20°C Transverse to Flow	70 - 90 μm/m.°C
Specific Heat Capacity	1.46 - 1.47 J/g.°C
Thermal Conductivity	0.19 - 0.24 W/m.K
Maximum Service Temperature, Air	41 - 103 °C
Melting Point	130°C
Vicat Softening Point	47 - 117 °C
Glass Temperature	**2** - 105 °C

2.7.5 Optical properties of PMMA:

PMMA exhibits very good optical properties – it transmits more light (up to 93% of visible light) than glass. Combined with its good degree of compatibility with human tissue, it can be used for replacement intraocular lenses or for contact lenses. Unlike glass, PMMA does not filter ultraviolet light. It transmits UV light down to 300 nm and allows infrared light of up to 2800 nm to pass.

Table 2.6 Optical properties of Polymethyl methacrylate.

Optical Properties	Value
Haze	1 - 96 %
Transmission, Visible	80 - 93 %
Refractive Index	2.1 - 1.498

2.7.6 Chemical resistance of PMMA:

Acrylics are unaffected by aqueous solutions of most laboratory chemicals, by detergents, cleaners, dilute inorganic acids, alkalis, and aliphatic hydrocarbons – however, acrylics are not recommended for use with chlorinated or aromatic hydrocarbons, esters, or ketones. It dissolves completely in chloroform, di- and trichlorethane, which is used for production of glues. The chemical resistance will vary with stress level, temperature, reagents and duration of exposure.

PMMA are physiologically harmless. Due to their low moisture absorption capacity they are not attacked by moulds and enzymes.

2.7.7 Processing methods of PMMA:

PMMA is suitable for injection moulding, extrusion, extrusion blow moulding (impact modified acrylics only), thermoforming, casting. The melt flow index of the material varies according to the method of treatment:

− Low melt flow index (0.8 – 2.5) – materials intended for extrusion;

− Medium melt flow index (2.5 - 10) – general-purpose PMMA;

− High melt flow index (> 10) – PMMA for injection moulding of products having a complex shape.

For injection moulding the mould temperature should be between 40 and 80°C, depending on the type, the material temperature should be between 200 and 250°C. Usually high injection pressures are needed because of poor flow properties. This is particularly important for optical mouldings where visible weld lines will form if the correct parameters are not used. During injection moulding internal stresses often build up,

which can be eliminated by heating at a temperature about 80°C (tempering).

Mould's nozzle is an important factor when manufacturing PMMA-product. The size of the nozzle gate varies depending on the shape and the size of the product. Products manufactured from PMMA are mainly clear and transparent and it is important that they do not have any scratches. So that it is recommend to use at least draft angle of 1° (rather 2°). Because PMMA has high viscosity, the gas removing channels can be quite deep, from 0.04 to 0.08 mm.

Misoperation due to higher temperature causes destruction of PMMA, accompanied by release of methylmethacrylate or other low-molecule volatile products. The process also leads to a loss of mass, which makes it undesirable, and a good knowledge of the thermo-physical properties of the polymer is necessary in order to avoid it, especially in the temperature range processing (220-250°C).

Acrylics are easily sawed, drilled, milled, engraved, and finished with sharp carbide-tipped tools. Cut surfaces may be readily sanded and polished. They are also readily bent or thermoformed at low temperature and solvent bonding of properly fitting parts produces a strong, invisible joint. PMMA can be welded by all the plastics welding processes such as hot-blade, hot-gas, ultrasonic or spin welding.

2.7.8 Disintegration of polymers:

Transparent and opaque (non-transparent) materials differ in effects of disintegration. Experimental data are useful in analyzing such effects in transparent amorphous and crystal materials. For simplest investigations, a Q-switch laser with regulated output power, lenses for beam focusing, a camera and investigated specimens are sufficient.

Special care should be taken to aberrations of the optical system and elements, and particularly to new classes of aberrations connected to high-power laser systems. Two mechanisms are recognized: formation of rounded pores and formation of almost flat cracks (fissures). It seems that the type of disintegration in investigated power range depends only on the focal length of a lens; pores appear with greater focal length. The zone of disintegration has a conical form with several dots as centers of scattering. Polystyrene and PMMA have similar behavior during the laser beam interaction. Of special interest is to observe the statistics of cracks formation. It is common to investigate the interaction with: low power (1-10 MW) and long focal length (50-{100 mm); high power (50-100 MW) and long focal length (50-100 mm); high power and short focal length (< 50 mm).

The influence of optical in homogeneity and impurities to the threshold and character of disintegration is important. Both the kinetics of disintegration and the measurements of stress open new fields of investigation. Optical techniques for measurements, like photoelasticity, holography and optical tomography, were developed a long time ago. The potential role of newly developed ps and fs laser spectroscopies increases. The schematic of a polymer photodestruction is presented in Figure 2.19 and could be the object for analysis in photochemistries. [Kovačević, A. et al. (2007)].
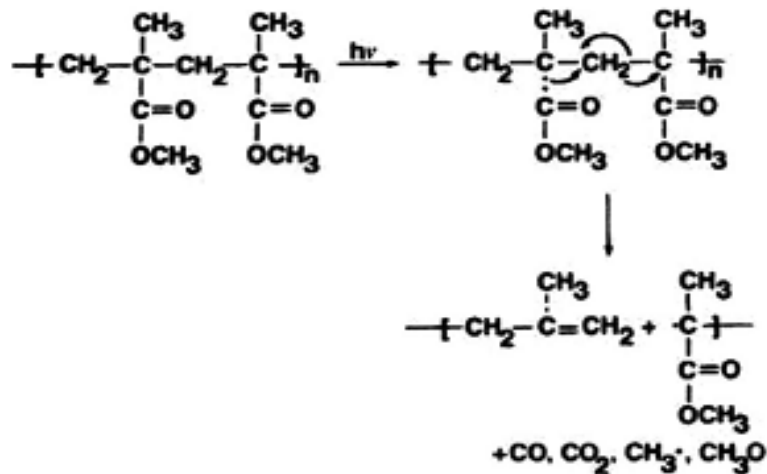
Figure 2.12: Some possible chain scissions of PMMA resist.

2.7.9 Applications of PMMA:

PMMA is an economical, versatile general-purpose material. It is available in extruded and/or cast material in sheet, rod and tube forms, as well as custom profiles. Various types of acrylics are used in a wide variety of fields and applications, including:

- Optics: Dust covers for hi-fi equipment, sun-glasses, watch glasses, lenses, magnifying glasses;

- Vehicles: Rear lights, indicators, tachometer covers, warning triangles; Electrical engineering: Lamp covers, switch parts, dials, control buttons; Office equipment: Writing and drawing instruments, pens;

- Medicine: Packaging for tablets, pills, capsules, suppositories, urine containers, sterilisable equipment;

- Others: Leaflet dispensers, shatter-resistant glazing, shower cubicles, transparent pipelines, illuminated signs, toys [Harper, John Wily& Sons (2005)].

2.8. The Laser :

Throughout the first half of the 20th century, the most commonly used light source for interferometry was a pinhole illuminated by a mercury arc through a filter which isolated the green line (λ=546 nm). Such a source gave only a very small amount of light with limited spatial and temporal coherence. The development of the laser made available, for the first time, an intense source of light with a remarkably high degree of spatial and temporal coherence and initiated a revolution in interferometry. The origins of the laser can be traced back to 1917, when Einstein pointed out that atoms in a higher energy state, which normally radiate spontaneously, could also be stimulated to emit and revert to a lower energy state when irradiated by a wave of the correct frequency. The most remarkable feature of this process was that the emitted photon had the same frequency, polarization, and phase as the stimulating wave and propagated in the same direction. Schawlow and Townes [1958] were the first to show that amplification by stimulated emission was possible in the visible region, and that a simple resonator consisting of two mirrors could be used for mode selection. The first practical laser was the pulsed ruby laser [Maiman, 1960]. Continuous laser action was achieved soon afterwards with the helium-neon laser, initially in the infrared [Javan, Bennett, and Herriot, 1961] and then in the visible region [White and Rigden, 1962]. The high degree of directionality and coherence of laser light were verified by Collins et al.[1960]. This was followed by the observation of interference fringes when the beams from two pulsed ruby lasers were superposed [Magyar and Mandel, 1963].

Lasers have removed most of the limitations of interferometry imposed by thermal sources and have made possible many new techniques. (P.Hariharan, (2003)).

2.8.1 Continuous-wave – millisecond – microsecond lasers

Continuous-wave (CW) and long-pulsed lasers are typically used to process materials either at a fixed spot (penetration material removal) or in a scanning mode whereby either the beam or the target is translated. Millisecond- and microsecond-duration pulses are produced by chopping the CW laser beam or by applying an external modulated control voltage. Fixed Q-switched solid-state lasers with pulse durations from tens of microseconds to several milliseconds are often used in industrial welding and drilling applications. Continuous-wave carbon dioxide lasers (wavelength $\lambda = 10.6$ µm and power in the kilowatt range) are widely employed for the cutting of bulk and thick samples of ceramics such as SiN, SiC, and metal-matrix ceramics (e.g. Duley, 1983). Continuous-wave laser radiation allows definition of grooves and cuts. On the other hand, low-power CO_2 lasers in the 10–150-W range are used for marking of wood, plastics, and glasses. Argon-ion lasers operating in the visible range (λ=419–514 nm) are utilized for trimming of thick and thin resistors. In the biomedical field various CW lasers have been used. For example, the CO_2 laser radiation is absorbed in the tissue within a layer of depth about 20 m, thus achieving a continuous ablation front. On the other hand, the Nd: YAG (λ=1064 nm) and argon-ion radiation penetration is of the order of millimeters, giving rise to explosive ablation events. Srinivasan et al.(1995) used an argon-ion laser operating in the UV ranges of 275–305 and 350–380 nm to ablate polyimide Kapton films. By chopping the laser beam to produce millisecond and microsecond pulses, they showed that the ablation process scales with an intensity threshold rather than the commonly used threshold. This is certainly not surprising, since, if the laser energy is spread over a long pulse, the beam intensity weakens and the induced temperature and structural and chemical response of the target may be of different nature.

In fact, Srinivasan (1992) showed that the etching of polymer films with long, millisecond–microsecond pulses leaves evidence of molten material and carbonization of the walls, although not indicative of the ablation process that characterizes nanosecond-pulse UV laser ablation. Microfabrication applications involving direct writing can be effected by CW Ar^+ and Kr^+ lasers, utilizing frequency-doubled lines. Highpower CW Nd : YAG lasers operating on the fundamental wavelength and on

frequencydoubled and -tripled harmonics are often used for various cutting and microprocessing applications (Costas,2009, pp.33-34).

2.8. 2. Femtosecond lasers:

Femtosecond laser micromachining has become increasingly important in recent years for many fields, including micro-optics, micro-electronics, micro-biology, and micro-chemistry. Laser ablation, because of its non-contact nature, allows the micromachining and surface patterning of materials with minimal mechanical and thermal deformation. It is now well known that for many of these applications, the femtosecond regime offers advantages over the nanosecond regime. These advantages lie in its ability to deposit energy into a material in a very short time period, before thermal diffusion can occur. As a result, the heat-affected zone, where melting and solidification can occur, is significantly reduced. Smaller feature sizes, greater spatial resolution, and better aspect ratios can hence be achieved.

Another advantage of femtosecond laser micromachining is its versatility in terms of both the materials that can be processed and the type of processing. A variety of materials have been demonstrated to be suitable for femtosecond laser micromachining, such as metals, semiconductors, polymers, oxide ceramics, silica aerogels, optical glasses, and crystals. A variety of processing methods have been used, including the fabrication of photonic crystals, waveguides, gratings and single mode couplers, and the storage of data [Zoubir et al., (2003)].

In the sub-picosecond or femtosecond regime, the laser pulse is shorter than the relaxation times, and the equilibrium assumption is no longer valid, necessitating treatment of the microscopic mechanisms of energy transfer via quantum mechanics. One notable characteristic of femtosecond lasers is the high radiation intensity that has the ability to

create high-density plasmas. On the other hand, by beating the thermal diffusion time scale, femtosecond-laser radiation can in principle be used for micromachining with minimal thermal damage to the surrounding area. In the UV range, KrF (λ=248 nm) excimer lasers with typical pulse duration 500 fs and pulse energies in the range several to tens of millijoules have been demonstrated in the processing of Al and glassy C (Sauerbrey et al., 1994), Ni, Cu, Mo, In, Au, W (Preuss et al., 1995), fused silica (Ihlemann, 1992), and ceramics such as Al_2O_3, MgO, and ZrO_2(Ihlemann et al., 1995), and for polymer ablation (Boret al.,1995; Wolff-Rottke et al.,1995). KrF excimer lasers have also been used in studies of high-density-gradient Al and Au plasmas (Fedosejevs et al., 1990) and for production of soft X-rays from Al (Teubner et al., 1993). The latter was also accomplished from Cu and Ta targets by near-IR Ti : sapphire-laser irradiation at λ=807 nm, with pulse duration 120 fs and pulse energy 60 mJ (Kmetec et al., 1992). A Ti: sapphire system with pulse duration of 150 fs andλ=770 nm was used in studies of gold ablation (Pronko et al., 1995), while pulse durations of 170–200 fs at wavelength λ = 798 nm and energy 4 mJ ablated polymers through a multiphoton ablation mechanism. Ti: sapphire-laser technology is often utilized in the laboratory environment and has recently made inroads into industrial applications, for example in the repair of lithographic masks. Amplified systems typically deliver 1-mJ near-IR pulses at maximum frequency 1 kHz. By utilizing stronger pumping lasers it is possible to extract pulses in the range tens of millijoules, albeit at reduced frequencies. On the other hand, the laser system could be configured to deliver microjoule or picojoule pulses at higher frequencies. Intense, visible dye-laser radiation (pulse duration 160 fs, λ=616 nm, energy 5 mJ) generated Si plasmas of high-energy-X-ray-emitting density (Murnane et al., 1989). In a biomedical application (Kautek et al., 1994),

a dye laser (pulse duration 300 fs, λ=615 nm, pulse energy > 0.18 mJ) produced high-quality ablation in human corneas, characterized by damage zones less than 0.5m wide. An interesting development in high-repetition-rate femtosecond-laser systems has been the development of (fiber) lasers that may give Megahertz repetition rates with hundreds of nanojoules per pulse or correspondingly pulse rates of∼100 kHz at tens of microjoules per pulse at λ=1,064 nm with pulse duration∼200 fs. Similar specifications have been achieved with disk or directly diode-pumped high-energy femtosecond oscillators. These lasers are utilized for film micromachining and the internal writing of optical waveguide structures in transparent materials [Costas,(2009)].

2.8.3.Physical mechanisms for femtosecond laser micromachining:

Femtosecond laser micromachining results from laser-induced optical breakdown, a process by which optical energy is transferred to the material, ionizing a large number of electrons that, in turn, transfer energy to the lattice. As a result of the irradiation, the material can undergo a phase or structural modification, leaving behind a localized permanent change in the refractive index or even a void.

During irradiation, the laser pulse transfers energy to the electrons through nonlinear ionization. For pulse durations greater than 10 fs, the nonlinearly excited electrons are further excited through phonon-mediated linear absorption, until they acquire enough kinetic energy to excite other bound electrons — a process called avalanche ionization. When the density of excited electrons reaches about 10^{29}m^{-3}, the electrons behave as a plasma with a natural frequency that is resonant with the laser — leading to reflection and absorption of the remaining pulse energy.

2.8.4. Laser Direct Writing (LDW) Process:

From the earliest work on laser interactions with materials, direct-write processes have been important and relevant techniques to modify, add, and subtract materials for a wide variety of systems and for applications such as metal cutting and welding. In general, direct-write processing refers to any technique that is able to create a pattern on a surface or volume in a serial or "spot-by-spot" fashion. This is in contrast to lithography, stamping, directed self-assembly, or other patterning approaches that require masks or preexisting patterns.

At first glance, one may think that direct-write processes are slower or less important than these parallelized approaches. However, direct-write allows for precise control of material properties with high resolution and enables structures that are either impossible or impractical to make with traditional parallel techniques. Furthermore, with continuing developments in laser technology providing a decrease in cost and an increase in repetition rates, there is a plethora of applications for which laser direct-write (LDW) methods are a fast and competitive way to produce novel structures and devices [Craig and Alberto, (2007)].

2.8.5. Lasers for materials processing:

Lasers, with their unique coherent, monochromatic, and collimated beamy characteristics, are used in ever-expanding fields of applications. Different applications require laser beams of different pulse duration and output power. Lasers employed for materials processing range from those with a high peak power and extremely short pulse duration to lasers with high-energy continuous-wave output.

2.8.6. Ultrafast-laser interactions with material (PMMA):

Lasers that can produce coherent photon pulses with durations in the femtosecond regime have opened up new frontiers in materials research with extremely short temporal resolution and high photon intensity. The ultrafast nature of femtosecond lasers has been used to observe, in real time, phenomena including chemical reactions in gases (Zewail,1994) and electron–lattice energy transfer in solids (Shah, 1996). On the other hand, ultra-short laser pulses impart extremely high intensities and provide precise laser-ablation thresholds at substantially reduced laser energy densities. The increasing availability of intense femtosecond lasers has sparked a growing interest in high-precision materials processing. In contrast to material modification using nanosecond or longer laser pulses, for which standard modes of thermal processes dominate, there is no heat exchange between the pulse and the material during femtosecond-laser–material interactions. [Backus, (1998)].

As a consequence, femtosecond laser pulses can induce nonthermal structural changes driven directly by electronic excitation and associated nonlinear processes, before the material lattice has equilibrated with the excited carriers. This fast mode of material modification can result in vanishing thermal stress and minimal collateral damage for processing practically any solid-state material. Additionally, damage produced by femtosecond laser pulses is far more regular from shot to shot. These breakdown characteristics make femtosecond lasers ideal tools for precision material processing. Thorough knowledge of the short-pulse-laser interaction with the target material is essential for controlling the resulting modification of the target's topography. The use of ultra-short pulses with correspondingly high laser intensities reduces the extent of heat diffusion into the target, facilitating instantaneous material

expulsion. This enables high-aspect-ratio cuts and features, free of debris and lateral damage (e.g. Momma et al., 1998; Pronko et al., 1995;Liu et al., 1997;Wu,1997). Therefore, the ablation process is stable and reproducible. As a result, the produced structure size is not limited by thermal or mechanical damage, i.e. melting, formation of burr and cracks, etc. Thus, the minimal achievable structure size is limited mainly by diffraction to the order of a wavelength (Korte et al., 1999). It has also to be recognized that ultrafast-laser pulses enforce high intensities that trigger nonlinear absorption effects that may dominate the interaction process. One of the most important repercussions is the efficient processings of transparent dielectrics, which has a number of applications, enabling for example three-dimensional binary-data storage (Glezer et al., 1996). [Wood R. W., (1944), Harrison G. R., (1949), Michelson A. A., *Astrophys, (1899)]*

Chapter Three
Experimental part

In this chapter a simple method to produce sub surface gratings on Poly (methyl methacrylate) (PMMA) with femtosecond laser, and then tracking Refractive Index had been presented with Interferometer and Mat lab program.

3.1. The material sample:

Poly (methyl methacrylate) (PMMA) sample with: thickness ~ 5mm, and area 20mm x 20mm.

3.2. Sample preparation:

Focused femtosecond laser at high repetition rate to induce localized microstructures inside transparent materials, due to nonlinear absorption at high peak power.

The irradiation of the PMMA sample sub surface has been done by means of Coherent Legend Ti: Sapphire laser facility generated horizontal linear polarized light, pulsed at a 1-kHz repetition rate, with pulse duration of 250 fs at a central wavelength of about 800 nm. The output beam from the system had laser pulse energy of 0.105 µJ in the Gaussian mode with a diameter of ~3mm. The schematic of the experimental setup is shown in Fig.1. The laser beam was attenuated by a diffractive optic attenuator and its frequency was doubled (SHG) by a BBO crystal, generating laser irradiation at 387nm wavelength A neutral density (ND) filter placed between the reflection mirrors achieved a smaller integrated flounce. The laser beam passed through two UV mirrors to reduce the residuals IR radiation. The laser beam was focused to ~8µm diameter by a 20X Nikon microscope objective with a 0.45 numerical aperture (NA), 10 mm focal length and long working distance

of 8 mm. The sample under study is mounted on a PC controlled. Aerotech x-y-z translation stage (ANT-25LV) of 2.5nm resolution and the fabrication process was viewed by a CCD Camera, the grating writing (scanning) speed is 1.25 mm/s. The experiments were performed by translating the sample along the x-direction so that the laser beam scribed parallel structures, line by line along x axis; the line to line spacing (grating period) is 40µm.

The experiments using PMMA samples involved main step of investigation: the sub surface Refractive Index modification by ultra short UV laser pulses. The structure depth is 200nm. The structural dimension created at fixed spacing with the fixed pulse energy, the translation speed is constant in all irradiation processes as well.
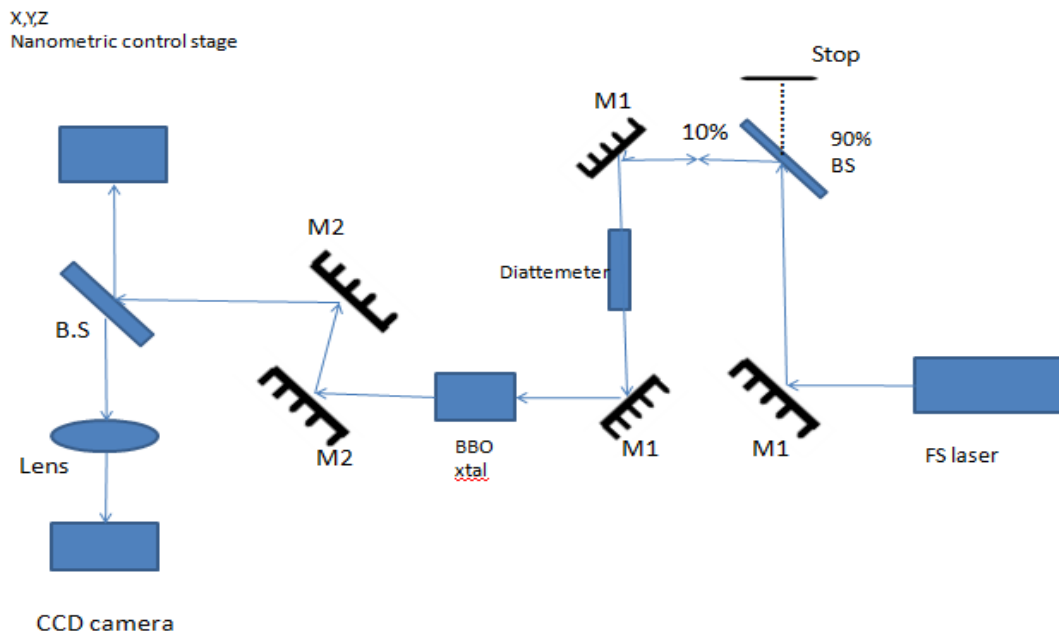

Figure 3.1 the experimental set up of sub surface irradiation technique, M_1 indicating to the IR irradiation part, M_2 indicating to the UV part (SHG) of irradiation after passing through BBO crystal.

Focused femtosecond laser to induce localized microstructures near the focal point of the laser beam inducing structural changes inside the transparent materials.
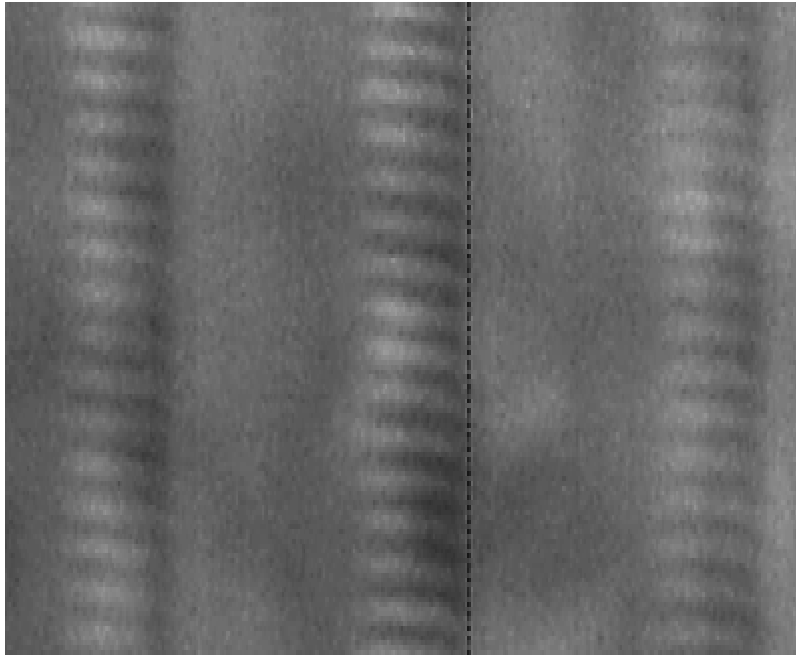
Figure 3.2. Fabrication of photonic structures.

The sample was translated with respect to the stationary writing laser beam, so that the structures were formed by overlapping pulses A single element of the diffraction grating was formed by a number of translated overlapping pulses, creating a "sub-structure", with a periodicity as shown in Figure 3.2. Each main vertical line is formed by overlapping ellipsoids generated by individual pulses.
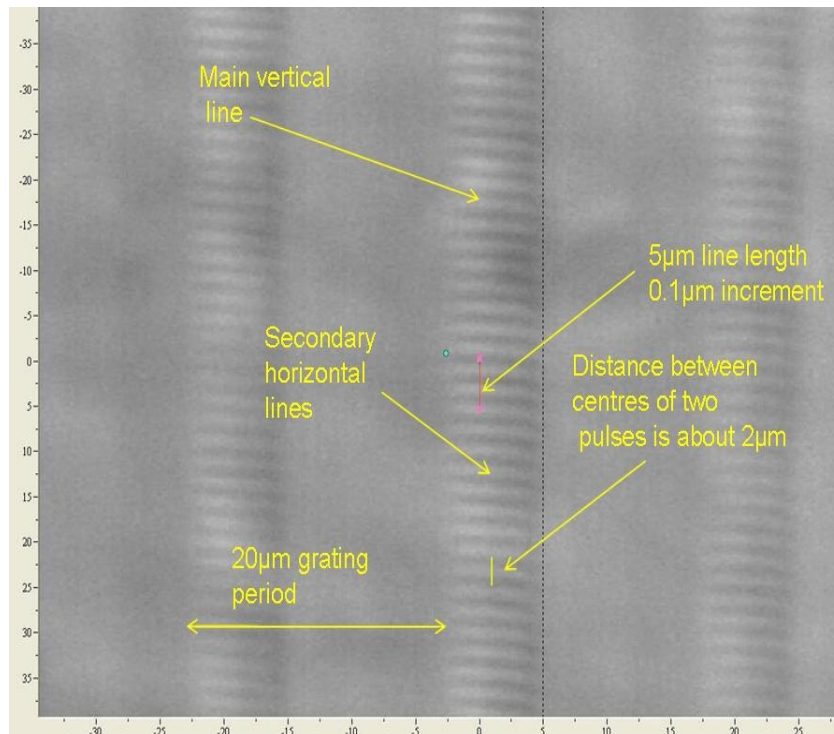
Figure 3.3. Microscope image of refractive index gratings using 50X objective written with UV 387nm laser irradiation

3.3. The sample Testing:

The irradiated and unirradiated Poly (methyl methacrylate) (PMMA) samples were inserted in the object arm of the interferometer the setup is as shown in fig.3. 2. is utilized for generating interference pattern. We used the coherent light source produced by a He-Ne laser, emitting on the 632 nm wavelength. Neutral density filters NDF1 and NDF2 were employed to control the laser intensity and to adjust fringe visibility (to get good fringe contrast). A 10× microscope objective (MO) of numerical aperture N.A=0.3 was placed after the sample to allow the desired magnification of the grating structure. By adjusting the position of microscope objective(MO) lenses it was possible to change the fringes widths at suitable beam intensity. A collimated and expanded reference wave interferes at small angle with the object wave transmitted by the

56

phase grating at the surface of a CCD camera (128×128 pixels), followed by frame grabber and PC. Then the interference fringes are recorded.
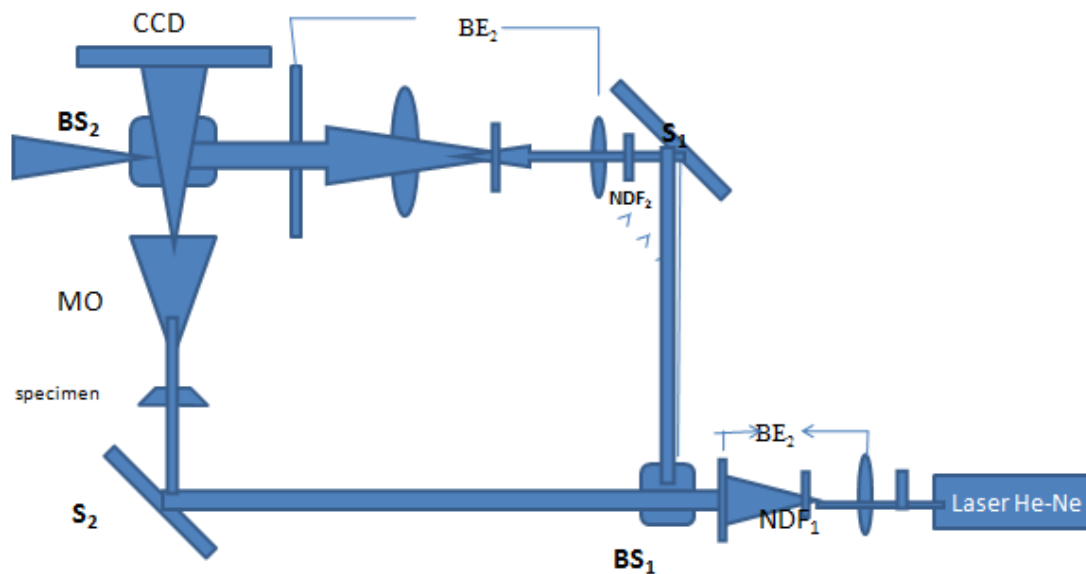
Fig.3.3 the experimental setup (Mach–Zehnder interferometric system in microscopic configuration. BS1 and BS2 are beam splitters. NDF1 and NDF2 are neutral density filters; BE1 a spatial filter and beam expander for the incident laser light; BE2 a spatial filter and beam expander to generate a plane wave front reference beam, and MO a microscope objective 10×.) with which we find the interference pattern for the samples.
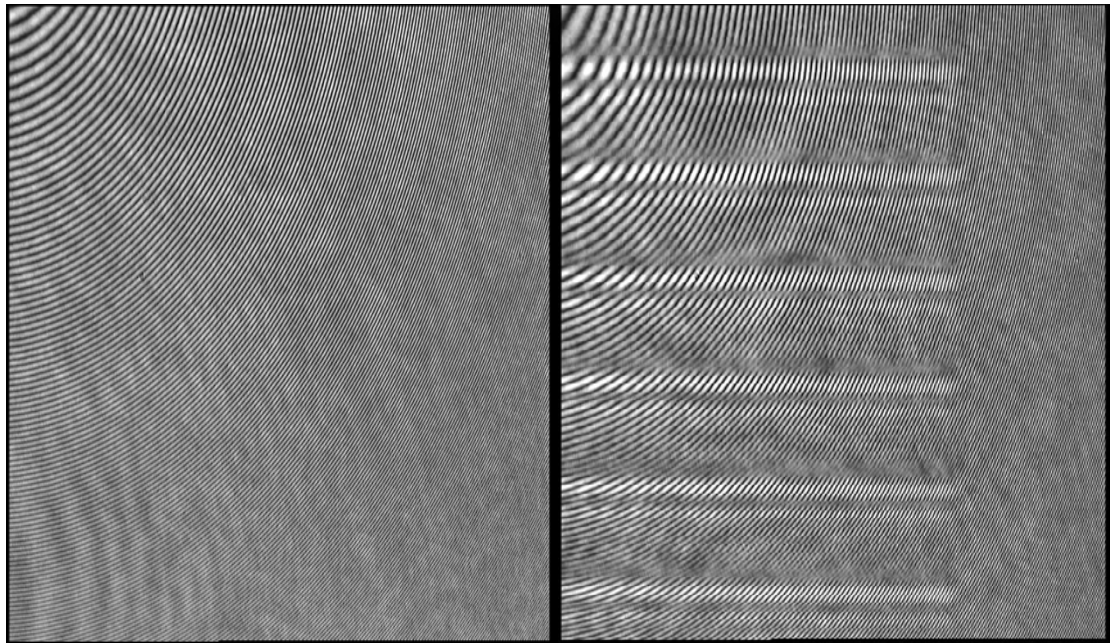
(a)   (b)

Fig.3.4: Interferometric patterns.

Interferometric patterns for the samples (a) before radiation and (b) after UV written phase grating with a scan speed of 1.25 mm/s, pulse energy of 0.105μJ.

The results of the experimental work will be summarized and presented in chapter four.

Chapter Four

Results and Discussion

The purpose of this chapter is to present and discuss the results of the experimental work in which the laser beam interact with PMMA samples, and then tracking the optical characterizations that occur using interferometric technique and mat lab.

4.1. Digitized interferogram of UV written phase gratings in PMMA:

The structural of Poly (methyl methacrylate) (PMMA) is modified by UV femto-second laser writing depth with 200nm, the dimension created at fixed spacing (40μm) with the fixed pulse energy, the fabrication process was viewed by a CCD Camera, the radiation change the optical characterization of PMMA sample, so this process lead the samples becomes as the gratings bulk since the scan in the periodic along x-axis.

The interferometer setup which the samples(before and after radiation) are inserted in, is utilized for generating interference pattern, the interference fringes are recorded by means of 128*128 pixels CCD camera, followed by frame grabber and PC.
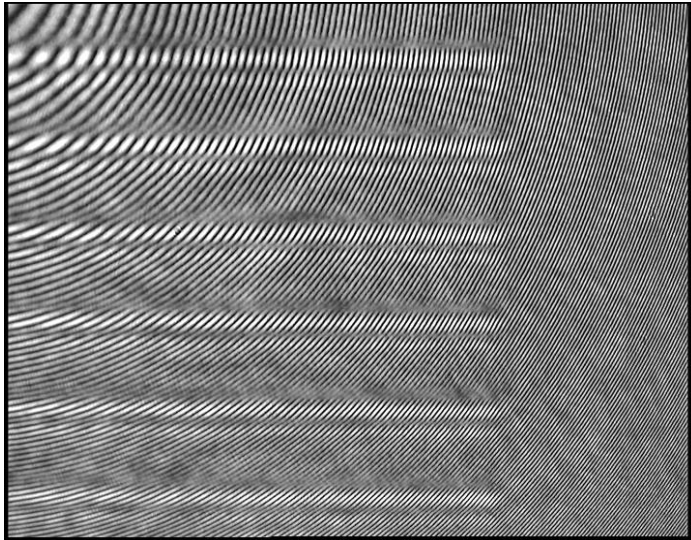
Figure 4.1. Digitized interferogram of UV written phase gratings in PMMA with a scan speed of 1.25 mm/s

Figure 4.1 show the interferometric pattern of the PMMA sample after UV laser written phase gratings with a scan speed of 1.25 mm/s, pulse energy of 0.105µJ, it is obvious from the image that the discontinuity of fringes pattern is due to the irradiated zones inside the sample, the interference fringe modifications in correspondence of irradiated zones across the sample surface.

4.2. Formation of a PMMA molecule:

To discus and investigate what happen inside the PMMA sample we can say there is photothermal and photochemical modifications, induced by the Ti: Sapphire laser, figure 4.2 shows the processes taking place inside the irradiated PMMA. It is obvious the effect of chain scission is essentially responsible for the producing of tiny volatile fragments, such as methyl or ester groups, etc., which easily escape the material surface. On the other hand, when free end-links are present in the irradiated material, the effect of cross-linking can take place. This effect is indicated by means of a formation of double C=C bonds in the backbone chain of the PMMA which originally contains only single C–C bonds.
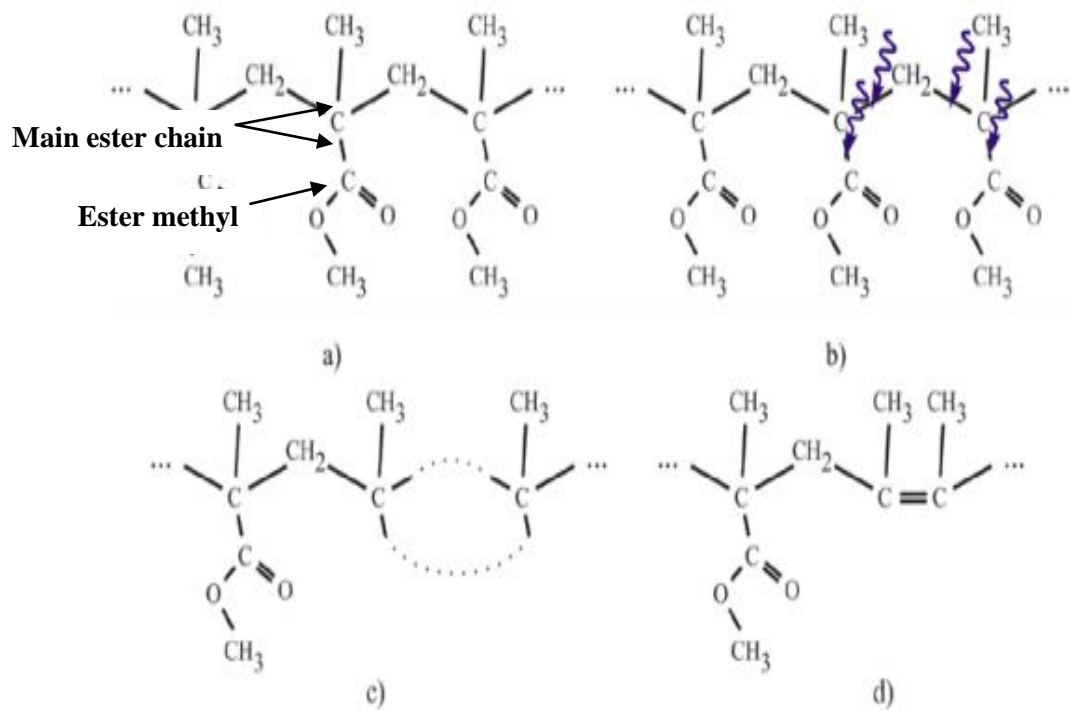
Figure4.2. Formation of a PMMA molecule with a double bond C=C; (a) unaffected PMMA molecule, (b) chain scission caused by incident radiation, (c) and (d) cross-linking.

4.3. Interferometric patterns and the corresponding refractive index map for the samples:
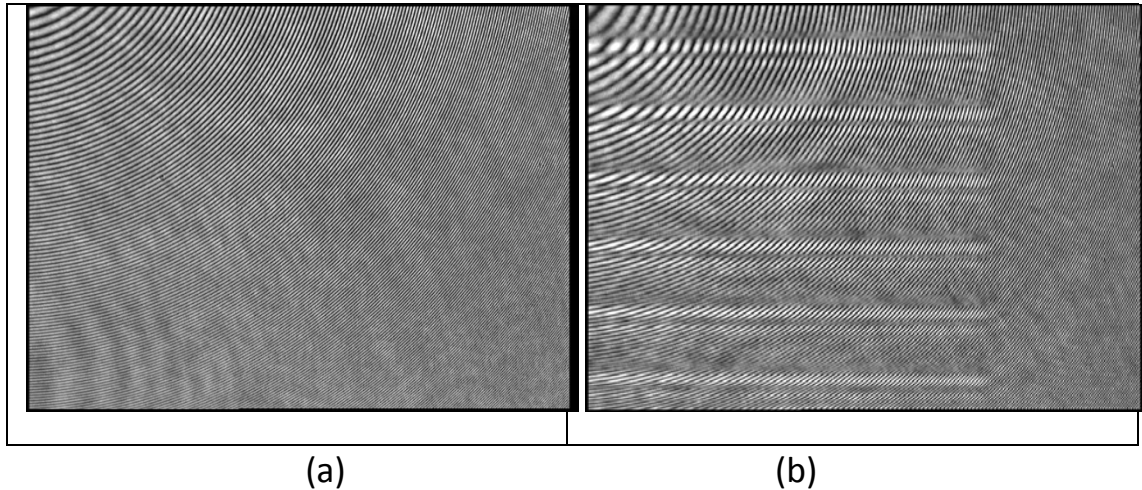
C01

<center>(a)   (b)</center>

Figure 4.3 Interferometric patterns for C01 samples (a) before radiation and (b) after UV written phase grating with a scan speed of 1.25 mm/s, pulse energy of 0.105μJ.
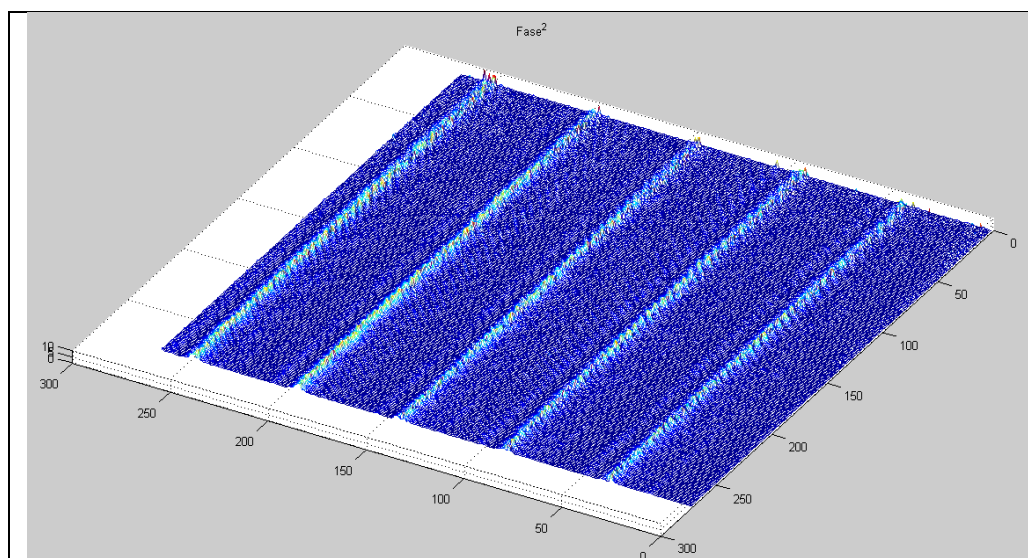

Figure 4.4 The corresponding refractive index map for interferometric patterns of C01sample (a) and (b).

The interference pattern recorded is shown in Fig.4.3. Fig.4.5. Fig.4.7. and Fig.4.9. (a) and (b) for all are the two digitized interferograms images (interferometric patterns), then subtracted with Matlab programme which mention in the Appendex to obtain the corresponding refractive index maps for the two interferometric patterns in Fig.4.4, Fig.4.6, Fig.4.8, and

<center>62</center>

Fig.4.10, with respectively, it is possible to observe the refractive index variation $\Delta n(x,y)$ from the phase change profile along x-axis for those figures, the high peek of Δn occurs at midpoint of focusing Coherent Legend Ti: Sapphire laser to PMMA sample.

C03

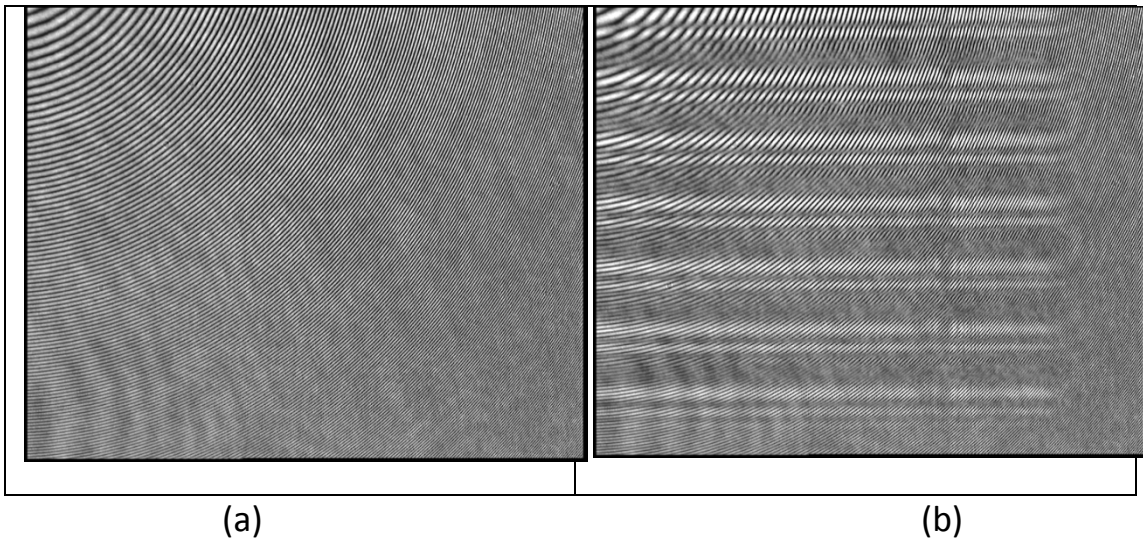(a)   (b)

Figure 4.5 Interferometric patterns for C03 samples (a) before radiation and (b) after UV written phase grating with a scan speed of 1.25 mm/s, pulse energy of 0.105μJ.

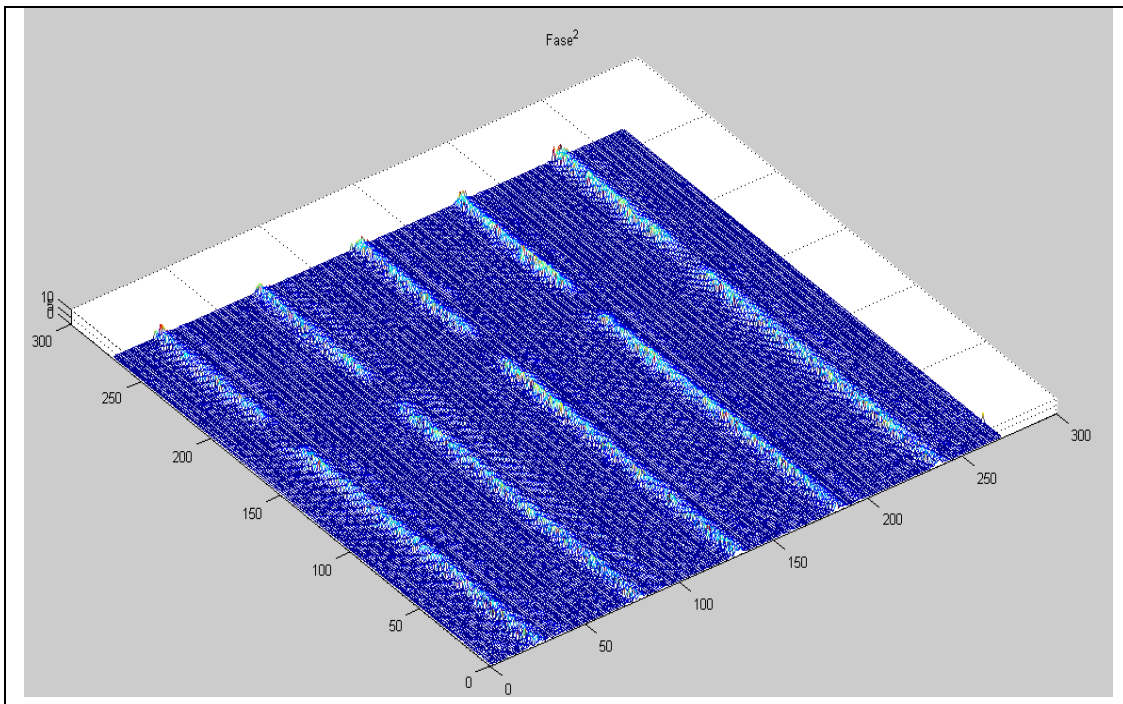Figure 4.6 The corresponding refractive index map for interferometric patterns of C03sample (a)   and (b).

Misura08

(a)   (b)

Figure 4.7 Interferometric patterns for Misura08 samples (a) before radiation and (b) after UV written phase grating with a scan speed of 1.25 mm/s, pulse energy of 0.105μJ.

Figure 4.8 The corresponding refractive index map for interferometric patterns of Misura08 samples (a) and (b).

Misura04

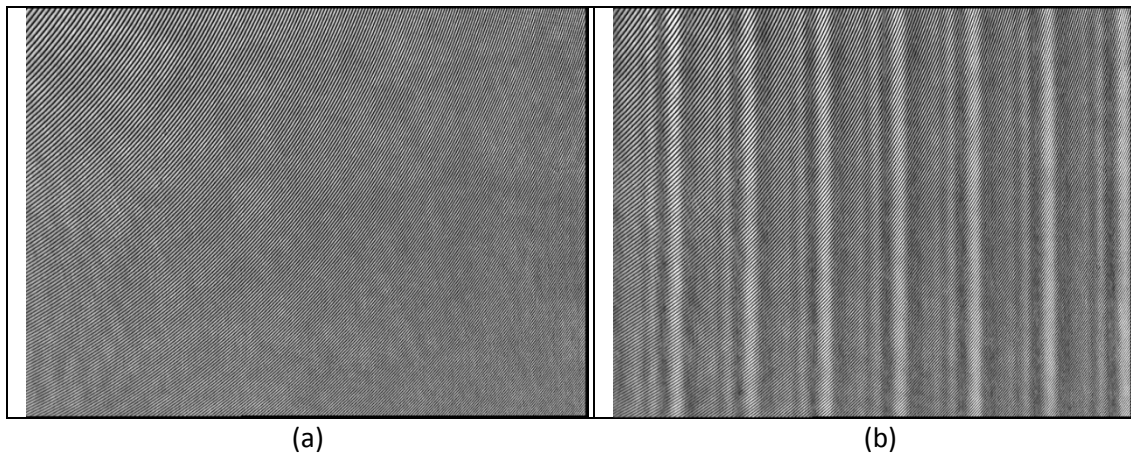(a)   (b)

Figure 4.9. Interferometric patterns for Misura04 samples (a) before radiation and (b) after UV written phase grating with a scan speed of 1.25 mm/s, pulse energy of 0.105μJ.

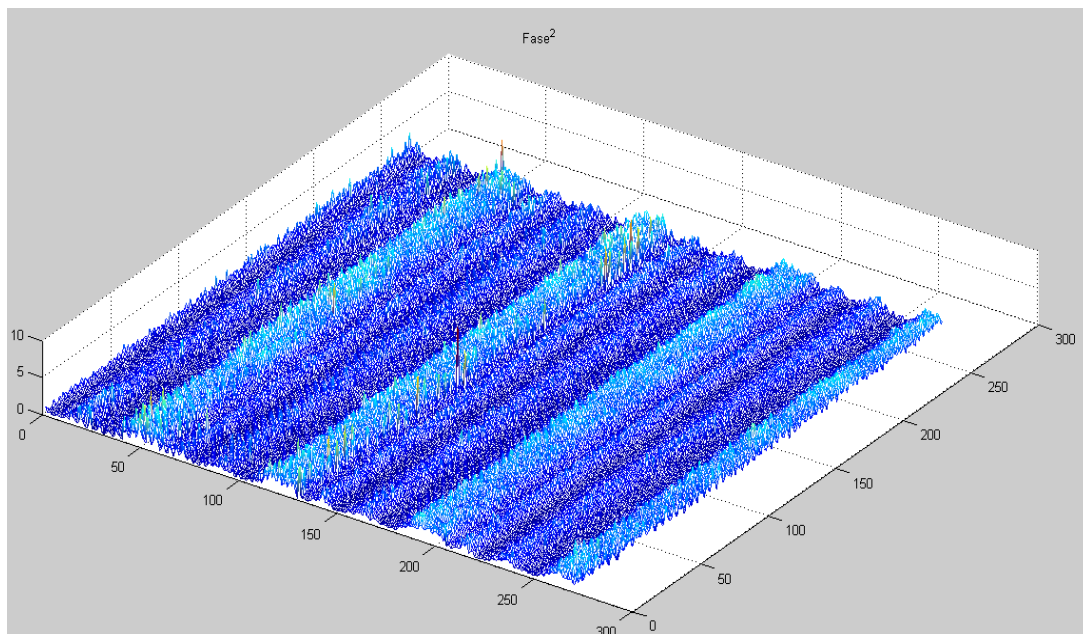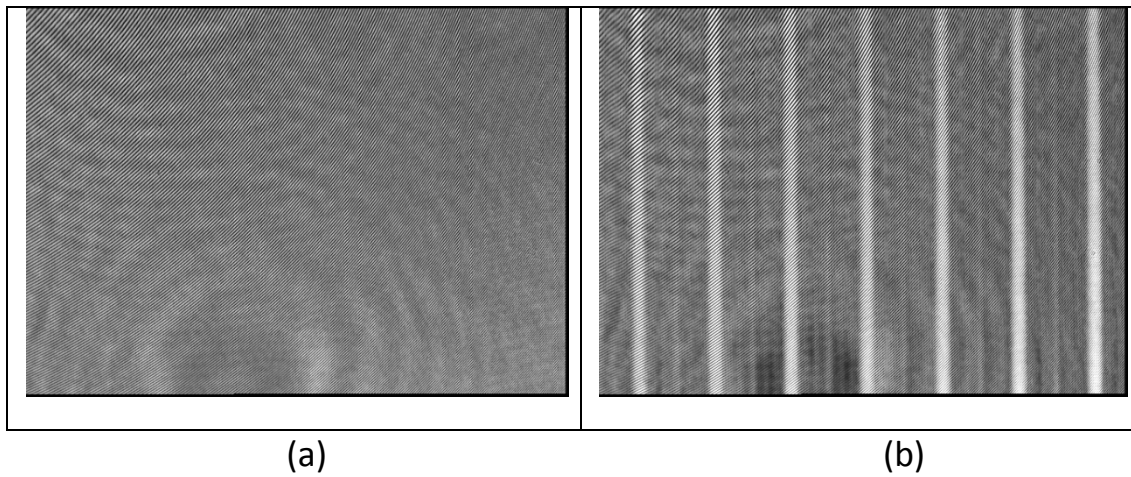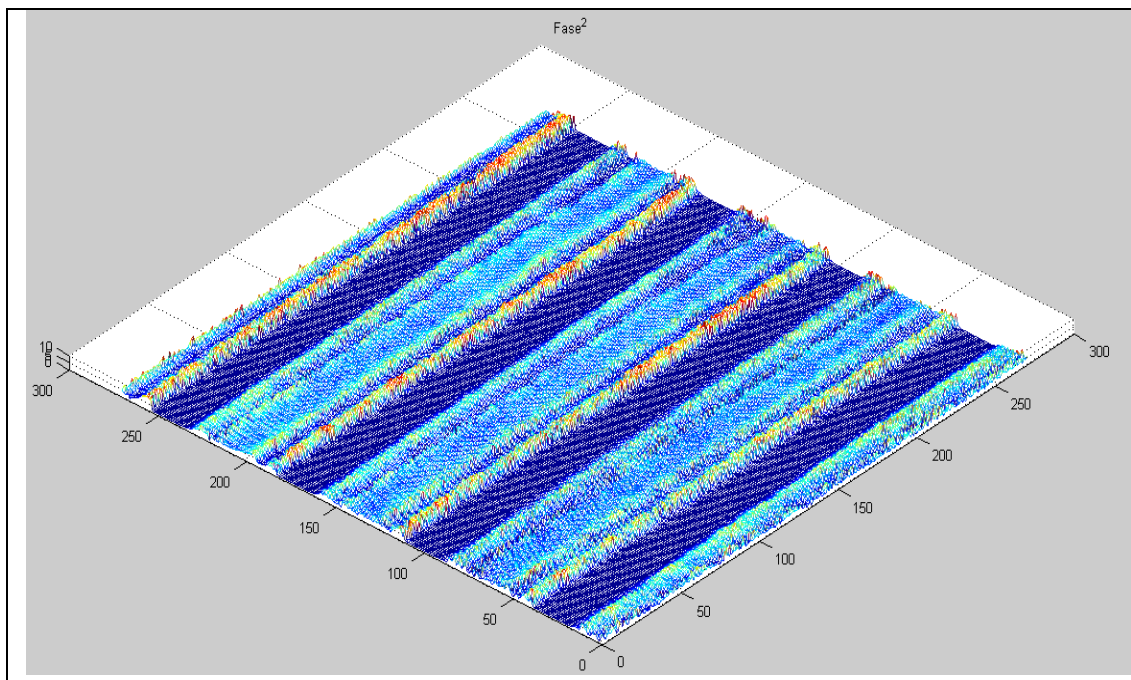Figure 4.10 The corresponding refractive index map for interferometric patterns of Misura04 samples (a) and (b).
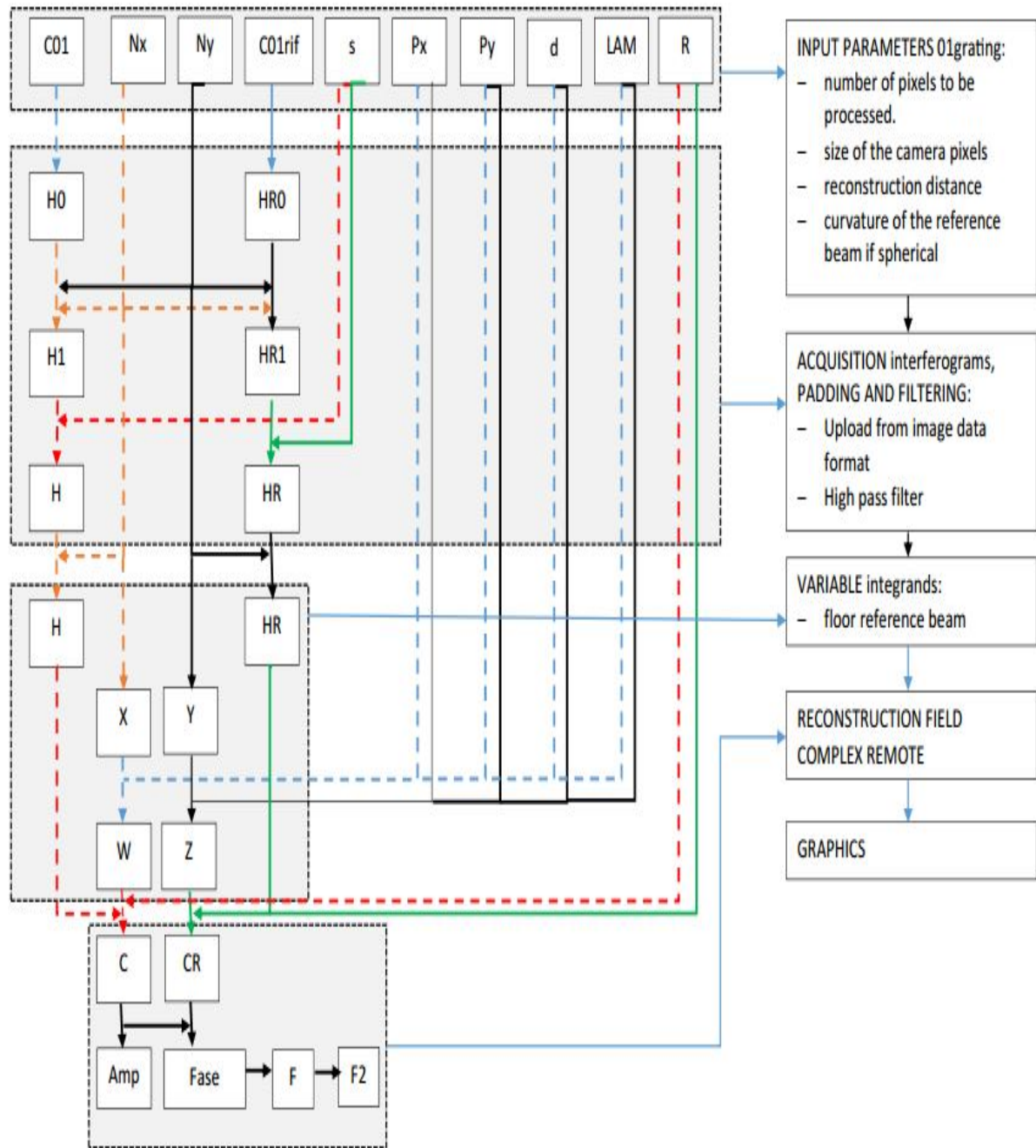
Flow chart:

Figure 4.11 the flow chart for the matlab program with which we find the corresponding refractive index.

4.4 Conclusions:

In conclusions the irradiation of the PMMA sample sub surface has been done by means of Coherent Legend Ti: Sapphire laser facility generated horizontal linear polarized light, pulsed at a 1-kHz repetition rate, with pulse duration of 250 f s at a central wavelength of about 800 nm. The output beam from the system had laser pulse energy of 0.105 µJ in the Gaussian mode with a diameter of ~3mm, the irradiated sub surface zone of the sample was modified by accumulated flounce and heat. Bragg type phase gratings are produced in bulk polymethyl methacrylate .

The change in the light intensity indicates a periodic change in the optical density which may be related to the laser induced total refractive index change independent of specific molecular bond changes.

It is observed that the discontinuity of fringes pattern is due to the irradiated zones inside the sample, the interference fringe modifications in correspondence of irradiated zones across the sample surface.

Decreases in this monomer content after laser irradiation, are related to main chain scission, molecular weight decrease and decreased refractive index.
Increases in monomer proportion indicate cross-linking and increased refractive index.

The usage of interference technique and matlab programme has been very sufficient to track the variation in Δn through the refractive index map.

4.5 Future work:

Further work to be presented include the investigation of temperature stability of the photo-induced gratings, UV-visible and FT infrared spectroscopic studies that illustrate the material modification mechanism, and the demonstration of grating structures written into single-mode and multimode plastic optical fibres.

Laser surface processing will continue to improve the performance of materials in existing applications and will open the door to new materials and novel applications that would not be possible without these unique processing capabilities.

Finally, the research presented here need to be extended to other classes of polymers including cross-linked elastomers, hydrogels, polyesters and polycarbonates. Developing Surface Modification from these polymers could be important in several applications.

References

1- Bass M., Van Stryland E. W., Williams D. R., and Wolfe W. L., "Handbook of Optics. Fundamentals, Techniques, and Design, Vol. 1," General Principles (pp. 146-149). New York: McGraw-Hill, Inc, 1995.

2- Backus, S., Durfee III, C. G., Murnane, M. M. & Kapteyn, H. C. *High power ultrafast lasers*. Rev. Sci. Instrum. 69,1207–1223 (1998).

3- Baum, A;Scully, P.J; Basanta, M; Thomas, C.I.P; Fielden P.R; Goddard, N.J. *Photochemistry of refractive index structures in poly(methyl methacrylate) by femtosecond laser irradiation*, Opt.Lett.[Online], 2007, 32, pp 190-192.

4- Baum, A; Scully, P.J; Perrie, W; Jones, D; Isaac, R; Jaroszynski. D.A. *Pulse-duration dependency of femtosecond laserrefractive index modification in poly(methyl methacrylate)*, *Opt.Lett*. [Online], **2008,***33*, pp 651-653.

5- Baum A., De Nicola S., Abdalah S., Al-Naimee K., Geltrude A., Locatelli M., (2011), "*Optical characterization of PMMA phase gratings written by a 387nm femtosecond laser*," Optics Communications, vol. 284, pp. 2771-2774.

6- Bloembergen, N. A brief history of light breakdown. J. Nonlinear Opt. Phys. 6,377–385 (1997). .

7- Bloembergen, N. Laser-induced electric breakdown in solids. IEEE J. Sel. Top. Quant. Electron. 10, 375–386 (1974). .

8- Brabec, T. & Krausz, F. Intense few-cycle laser fields: Frontiers of nonlinear optics. Rev. Mod. Phys. 72,545–591 (2000). .

9- Buividas, R. et al. (2012) *Femtosecond Laser Processing a new Enabling Technology*. Lithuanian Journal of Physics, Vol. 52,No. 4, pp. 301–311.

10- Cheng, J. (2004) *Direct-write Laser Micromachining and Universal Surface Modification of PMMA for Device Development*. Sensors and ActuatorsB99, 186-196.

11- Chimmalgi, A., Choi, T. Y., Grigoropoulos, C. P. & Komvopoulos, K. Femtosecond laser aperturless near-field nanomachining of metals assisted by scanning probe microscopy. Appl. Phys. Lett. 82,1146–1148 (2003). .

12- Clough, R. L., and S. W. Shalaby, (1991), eds. *Radiation Effects on Polymers*. American Chemical Sosiety, Washington, D. C., vol 475.

13- Costas, P. G. (2009) Transport in Laser Microfabrication. Cambridge: Cambridge University Press.

14- Craig, B. A. & Piqué, A., (2007) Laser Direct-Write Processing. MRS BULLETIN.VOLUME 32. JANUARY.

15- Dausinger, F., Lichtner, F. & Lubatschowski, H. Femtosecond Technology for Technical and Medical Applications(Springer, Berlin, 2004). .

16- Davis K. M., Miura K., Sugimoto N., and Hirao K., Opt. Lett.21, 1729 (1996).

17- Deepak, K.L.N.,, Venugopal S., & Narayana R. D., (2011) Femtosecond laser micro fabrication in polymers towards memory devices and microfluidic applications. Laser-Induced Damage in Optical Materials, Proc. of SPIE Vol. 8190.

18- Della Valle G., Osellame R., Chiodo N., Taccheo S., Cerullo G., Laporta P., Killi A., Morgner U., Lederer M., and Kopf D., Opt. Express13, 5976 (2005).

19- Du, D., Liu, X., Korn, G., Squier, J. & Mourou, G. Laser-induced breakdown by impact ionization in SiO_2 with pulse widths from 7 ns to 150 fs. Appl. Phys. Lett. 64,3071–3073 (1994). .

20- Florea, C. & Kim A. (2003) *Fabrication and Characterization of Photonic Devices Directly Written in Glass Using Femtosecond Laser Pulses*. JOURNAL OF LIGHTWAVE TECHNOLOGY, VOL. 21, NO. 1, JANUARY.

21- Graham, D. M., Martin, A. & Michael, J. W., (2006) *Direct laser written waveguide–Bragg gratings in bulk fused silica*. OPTICS LETTERS / Vol. 31, No. 18 / September 15. .

22- Hariharan P., " Optical Interferometry" (2003) Elsevier Science, Suite 1900, San Diego, CA 92101-4495, USA.

23- Harper, C. A. (2005) *Handbook of Plastic Processes*. John Wiley & Sons.

24- Harrison G. R., *J. Opt. Soc. Amer.*, **39** (1949), 522.

25- Horn, W. et al. (2012) *Electro-optical tunable waveguide Bragg gratings in lithium niobate induced by femtosecond laser writing*. Vol. 20, No. 24 / OPTICS EXPRESS 26925.

26- Homoelle, D., S. Wielandy, A.L. Gaeta, N.F. Borrelli, C. Smith, 1999. Opt. Lett., 24: 1311.

27- Htoo, M. S., ed. *Microelectronic Polymers*. Marcel Dekker, New York, 1989.

28- Itoh K., Kobayashi K. F., Ostendorf A., Sugioka K., Proc. of SPIE Vol. 5662 (SPIE, Bellingham, WA.

29- Joglekar, A. P. et al.A study of the deterministic character of optical damage by femtosecond laser pulses and applications to nanomachining. Appl. Phys. B 77,25–30 (2003). .

30- Kallepalli, L. N. D., Soma, V. R. & Desai, N. R. (2012) *Femtosecond-laser direct writing in polymers and potential applications in microfluidics and memory devices.* Optical Engineering (July 2012) 51(7), 073402. .

31- Kazuyoshi, I., (2006) Laser microengineering of photonic devices in glass. JLMN-Journal of Laser Micro/Nanoengineering, Vol. 1, No.1.

32- Keller, U. Recent developments in compact ultrafast lasers. Nature 424,831–838 (2003). .

33- Kip D., Appl. Phys. B 67 (1998) 131.

34- Kovačević, A. et al. (2007) Laser–PMMA Interaction and Mechanical Stresses. ACTA PHYSICA POLONICA A No. 5, Vol. 112.

35- Kro, D. M. et al. (2004) Fs-Laser Fabrication of Photonic Structures in Glass: the Role of Glass Composition. Fifth International Symposium on Laser Precision Microfabrication, Edited by I. Miyamoto, H. Helvajian,

36- Kruger, J. & Kautek, W. in Polymers and LightVol. 168 (ed. Lippert, T.) 247–289 (Springer, Berlin, 2004). .

37- Liu J. R., Zhang Z. Y., Chang S. D., Flueraru C., and Grover C. P., Opt. Commun.253, 315 (2005).

38- Liang, S; Scully, P.J; Schille, J; Vaughan, J; Benyezzar, M; Liu, D; Perrie. W. Writing parameters for 3D refractive index structures in polymethyl methacrylate using femtosecond radiation at 400 nm, J. Opt., (2002). A. 4: 105.

39- Max Born and Wolf, "Principles of Optics" *Electromagnetic Theory of Propagation, Interferece and Diffraction of Light*, 7th (expanded) edition, London, (2003).

40- Michelson A. A., *Astrophys. J.*, **8** (1899), 37; *Proc. Amer. Acad. Arts., Sci.*, **35** , 109.

41- Miura, K., J. Qiu, H. Inouye, T. Mitsuyu, K. Hirao, 1997. Appl. Phys. Lett., 71: 3329.

42- Oliveira, V. et al. (2012) Laser surface patterning using a Michelson interferometer and femtosecond laser radiation. Optics & Laser Technology 44, 2072–2075.

43- Pal, Bishnu P. (1992). *Fundamentals of Fibre Optics in Telecommunication and Sensor Systems*. New Delhi: New Age International. p. 663 (read section 3). ISBN 8122404693.

44- Pronko, P. P. et al.Machining of submicron holes using a femtosecond laser at 800-nm. Opt. Commun. 114,106–110 (1995).

45- Qiu, J., C. Zhu, T. Nakaya, J. Si, F. Ogura, K. Kojima, K. Hirao, 2001. Appl. Phys. Lett., 79: 3567.

46- Qiu, J., P.G. Kazansky, J. Si, K. Miura, T. Mitsuyu, K. Hirao, A.L. Gaeta, 2000. Appl. Phys. Lett., 77: 1940.

47- Saliminia A., N. T. Nguyen, M. C. Nadeau, S. Petit, S. L. Chin, and R. Vallee, J. Appl. Phys.93, 3724 (2003).

48- Scully, P.J; Jones, D; Jaroszynski, D.A. *Femtosecond laser irradiation of polymethylmethacrylate for refractive index gratings*, 49- J.Opt.A: Pure Appl. Opt. [Online], 2003, 5, pp S92-S96

49- Shyam Singh, " *Refractive Index Measurement and its Applications,"*Physica Scripta. Vo1, 65, 167-180, 2002.

50- Steinmeyer, G., Sutter, D. H., Gallmann, L., Matuschek, N. & Keller, U. Frontiers in ultrashort pulse generation: Pushing the limits in linear and nonlinear optics. Science 286,1507–1512 (1999). .

51- Stuart, B. C. et al.Nanosecond-to-femtosecond laser-induced breakdown in dielectrics. Phys. Rev. B 53,1749–1761 (1996). .

52- Stuart, B. C., Feit, M. D., Rubenchik, A. M., Shore, B. W. & Perry, M. D. Laser-induced damage in dielectrics with nanosecond to subpicosecond pulses. Phys. Rev. Lett. 74,2248–2251 (1995). .

53- Taleb, A. M. et al. (2011) Nanostructure Formation in Silicon Photovoltaic Cells by Femtosecond Laser Pulses . Materials Science Forum Vol. 670 pp 118-12.

54- Taranu A., Scully P., Al Naimee K., Vaughan J., and Baum A., (2010) *"Raman Mapping of Femotosecond Laser Written Photonic Structures inPolymethymethacrylate,"* in Proceedings of POF.

55- Thompson, L. F., C. G. Willson, and J. M. J. Frechet., eds. *Materials for Microlithography*; Radiations-sensitive Polymers. American Chemical Society, Washington, D. C., 1984, vol. 266.

56- Vishnubhatla, K.C. et al. (2008) *Inscription and characterization of micro-structures in silicate*, FOTURAN^{TM} and tellurite glasses by femtosecond laser direct writing. Commercial and Biomedical Applications of Ultrafast Lasers VIII, Proc. of SPIE Vol. 6881.

57- Wood R. W., *Nature*, **140** (1937), 723; *J, Opt. Soc. Amer.*, **34** (1944), 509; H Babcock, *ibid.*, **34** (1944), 1.

58- Wong W. H., Pun E. Y. B., and Chan K. S., IEEE Photon. Technol. Lett.15, 1731 (2003).

59- Yliniemi S., Albert J., Wang Q., and Honkanen S., Opt. Express14, 2898 (2006).

60- Zoubir, A. et al. (2003) Practical uses of femtosecond laser micro-materials processing. Appl. Phys. A 77, 311–315.

61- Zoubir, A. et al. (2004) Femtosecond laser fabrication of tubular waveguides in poly(methyl methacrylate). OPTICS LETTERS / Vol. 29, No. 16 / August 15.

Appendix

<u>Mat lab:</u>

The Matlab program with which we find the variation in the Refractive Index that happen after the PMMA sample was irradiated.

```matlab
clear all;

close all;


%%%INSERIMENTO PARAMETRI01grating


LAM = 0.6328;%lunghezza d'onda

Nx = 720;%numero di pixel da elaborare

Ny = 576;%numero di pixel da elaborare

Px = 8.16;%dimensione x pixel della telecamera

Py = 8.75;%dimensione y pixel della telecamera

d = 150000;%distanza di ricostruzione

% r = xx;%curvatura del fascio di riferimento se
sferico



%%%ACQUISIZIONE INTERFEROGRAMMI, PADDING E
FILTRAGGIO


%%Carica dati da formato immagine

H0 = imread('C01','bmp');

HR0 = imread('C01rif','bmp');
```

```matlab
H1 = double(H0(1:Ny,1:Nx));

HR1 = double(HR0(1:Ny,1:Nx));


% %Nessun filtro

% H = H1;

% HR = HR1;


% %Sottrazione media

% Hm = mean2(H1);

% HRm = mean2(HR1);

% H = H1-Hm*ones(Ny,Nx);

% HR = HR1-HRm*ones(Ny,Nx);


%Filtro passa alto

s = -(1/9)*[1 1 1; 1 -8 1; 1 1 1];

H = conv2(double(H1),double(s),'same');

HR = conv2(double(HR1),double(s),'same');


% %Filtro finestra Hamming

% Hd = zeros(41,41);

% Hd(4:37,4:37) = 1;

% Hd(18:22,18:22) = 0;

% s = fsamp2(Hd);

% % s = fwind1(Hd,hamming(41));

% H = conv2(double(H1),double(s),'same');
```

```matlab
% HR = conv2(double(HR1),double(s),'same');



%%%VARIABILI INTEGRANDE


H = H(8:Ny-8,10:Nx-10);

HR = HR(8:Ny-8,10:Nx-10);

[X,Y] = meshgrid(-(Nx-2)/2+9:(Nx-2)/2-9,-(Ny-2)/2+7:(Ny-2)/2-7);

R = 1;%fascio di riferimento piano

% R = exp(1i*pi/(LAM*r)*(X.^2*Px^2+ Y.^2*Py^2));%fascio di riferimento sferico

W = exp(1i*pi/(LAM*d)*(X.^2*Px^2+ Y.^2*Py^2));

Z = 1/(1i*LAM*d)*exp(1i*2*pi*d/LAM)*exp(1i*pi*LAM*d*(X.^2/((Nx)^2*Px^2) + Y.^2/((Ny)^2*Py^2)));



%%%RICOSTRUZIONE CAMPO COMPLESSO A DISTANZA d


C = Z.*fftshift(fft2(R.*H.*W));

CR = Z.*fftshift(fft2(R.*HR.*W));

Amp = abs(C);

Fase = angle(C./CR);

F=Fase(250:520,350:620);

F2=F.^2;
```

```matlab
%%%GRAFICI

figure(1);
imagesc(Amp);
shading interp;
% colormap('gray');
title('Ampiezza');

figure(2);
imagesc(Fase);
shading interp;
% colormap('gray');
title('Fase');

figure(3);
mesh(F2);
shading interp;
% colormap('gray');
title('Fase^2');
%figure(4);
 %subplot(1,2,1);
 %a = fftshift(fft2(H1));
%imagesc(real(a));
 %shading interp;
 %colormap(gray);
```

```
%title('fft ologramma');

%subplot(1,2,2);

%b = fftshift(fft2(H));

%imagesc(real(b));

%shading interp;

%colormap(gray);

%title('fft ologramma filtrato');
```

INSERIMENTO PARAMETRI01grating	INPUT PARAMETERS 01grating
numero di pixel da elaborare	number of pixels to be processed
dimensione x pixel della telecamera	size of the camera pixels
distanza di ricostruzione	reconstruction distance
curvatura del fascio di riferimento se sferico	curvature of the reference beam if spherical
ACQUISIZIONE INTERFEROGRAMMI, PADDING E FILTRAGGIO	ACQUISITION interferograms, PADDING AND FILTERING
Carica dati da formato imagine	Upload from image data format
Nessun filtro	No filter
Filtro passa alto	High pass filter
Filtro finestra Hamming	Hanning window filter
VARIABILI INTEGRANDE	VARIABLE integrands
fascio di riferimento piano	floor reference beam
RICOSTRUZIONE CAMPO COMPLESSO A DISTANZA d	RECONSTRUCTION FIELD COMPLEX REMOTE d
GRAFICI	GRAPHICS
fase	phase